

Optical remote sensing of debris covered glaciers

K. A. Casey et al.

This discussion paper is/has been under review for the journal The Cryosphere (TC).
Please refer to the corresponding final paper in TC if available.

Characterization of glacier debris cover via in situ and optical remote sensing methods: a case study in the Khumbu Himalaya, Nepal

K. A. Casey¹, A. Kääb¹, and D. I. Benn^{2,3}

¹Department of Geosciences, University of Oslo, P.O. Box 1047 Blindern, 0316 Oslo, Norway

²Department of Geography, University of St. Andrews, St. Andrews, UK

³The University Centre in Svalbard (UNIS), P.O. Box 156, 9171 Longyearbyen, Norway

Received: 28 November 2010 – Accepted: 22 January 2011 – Published: 7 February 2011

Correspondence to: K. Casey (k.a.casey@geo.uio.no)

Published by Copernicus Publications on behalf of the European Geosciences Union.

Title Page

Abstract Introduction

Conclusions References

Tables Figures

◀ ▶

◀ ▶

Back Close

Full Screen / Esc

Printer-friendly Version

Interactive Discussion



Abstract

Field spectrometry and physical samples of debris, snow and ice were collected from the ablation zones of Ngozumpa and Khumbu glaciers of the Khumbu Himalaya, Nepal in November and December 2009. Field acquired spectral reflectances and mineral and chemical composition of samples were used as ground truth for comparison with satellite optical remote sensing data. Supraglacial debris was characterized by several optical remote sensing methods, including hyperspectral reflectance analysis, multi-spectral band composites and indices, spectral angle relationships, thermal band temperature and emissivity analysis, as well as repeat image derived glacier velocity and theoretical supraglacial particle transport. Supraglacial mineral components were identified and mineral abundances were estimated on Khumbu Himalayan glaciers. Mass flux was estimated by false color composites and glacier velocity displacement fields. Supraglacial temperatures were compared with mineral abundances, implying potential parameters to estimate differential melt. Overall, glaciologic implications of debris cover characterizations are applicable to (1) glacier energy balance, (2) glacial kinematics and (3) mapping glacial extent. The methods presented can be used in synergy to improve supraglacial debris quantification and reduce errors associated with debris covered ice extent mapping, surface radiative properties, as well as debris covered ice mass flux and loss estimations.

1 Context

Many of the world's alpine glaciers have moderate to significant debris cover in their ablation zones, and this debris remains a challenge in optical satellite remote sensing glacier description. Previous optical remote sensing analysis of debris covered glaciers has largely focused on mapping glacial extent. While mapping "clean" bare glacier ice extent can be done quite successfully (Hall et al., 1988), even on a semi-automated basis (Paul et al., 2007); strategies for debris covered glacier extent mapping remain

TCD

5, 499–564, 2011

Optical remote sensing of debris covered glaciers

K. A. Casey et al.

Title Page

Abstract

Introduction

Conclusions

References

Tables

Figures

◀

▶

◀

▶

Back

Close

Full Screen / Esc

Printer-friendly Version

Interactive Discussion



in development and commonly utilize geomorphometric approaches (Taschner and Ranzi, 2002; Paul et al., 2004; Bolch et al., 2007; Buchroithner and Bolch, 2006; Shukla et al., 2010). A recent advance by Atwood et al. (2010) and Strozzi et al. (2010) involves the use of phase coherence between repeat synthetic aperture radar (SAR) data to delineate debris covered areas.

In addition to mapping glacier extent, glaciologic thermal properties as well as kinematic processes can be derived from optical remote sensing of glacier debris. Minimal to moderate glacier debris cover enhances ice and snow melt rates (Warren and Wiscombe, 1980; Oerlemans et al., 2009) while extensive debris cover – typical of several Himalayan glaciers – can insulate ice and dampen melt processes (Ostrem, 1959; Fujii, 1977; Mattson et al., 1993; Adhikary et al., 2000; Takeuchi et al., 2000; Nicholson and Benn, 2006). Ablation rates, melt water discharge (Mattson, 1990, 2000), and debris-cover regulated backwasting (Nakawo et al., 1999), are among the glaciologic variables that are affected by debris cover. Further, lithologic supraglacial patterns reveal the kinematic history of a debris covered glacier. Evidence of past surges and flow processes can be suggested by looped and folded moraines, as well as band and wave ogive patterns (Post and LaChapelle, 2000). Debris mantle patterns and assemblages indicate slope processes such as rock or ice falls or avalanches (Benn and Evans, 2010) as well as glacier flow regimes which can be described by glacial movement that is continuous, pulsed or of surge type (Kääb, 2005). Of course, flow dynamics from accumulation to ablation zones are complex and cannot be determined solely by surface optical remote sensing methods. However, inspecting supraglacial lithology can highlight distinct geologic sources in the accumulation zone which then reemerge supraglacially in the ablation zone, for example, giving an indication of englacial transport as well as the amount of debris transported.

Optical remote sensing multi-temporal image matching of debris cover can be utilized to estimate glacier velocities and theoretical surface particulate flow (Kääb et al., 1998; Frauenfelder and Kääb, 2000; Kääb, 2005). The synergy of glacier velocity and streamline information with supraglacial debris characterization can provide first-order

Optical remote sensing of debris covered glaciers

K. A. Casey et al.

Title Page

Abstract

Introduction

Conclusions

References

Tables

Figures



Back

Close

Full Screen / Esc

Printer-friendly Version

Interactive Discussion



Optical remote sensing of debris covered glaciersK. A. Casey et al.

[Title Page](#)[Abstract](#)[Introduction](#)[Conclusions](#)[References](#)[Tables](#)[Figures](#)[⏪](#)[⏩](#)[◀](#)[▶](#)[Back](#)[Close](#)[Full Screen / Esc](#)[Printer-friendly Version](#)[Interactive Discussion](#)

thermal- and kinematic-related glacier records of years, decades or centuries. Consideration of glacier transport and mass loss is relevant to glacier mass balance estimations at regional and global scales. Colloquially referred to as Earth's 3rd pole (Yao, 2010), the Himalayan glaciers are characterized by extensive debris cover. Sustained and widespread mass loss of ice in the Himalayas and in other regions can lead to crustal uplift (Tamisiea et al., 2001; Larsen et al., 2005), and of course, ultimately, sea level rise (Meier et al., 2007). Attention to and improved mapping of debris covered glaciers on a global scale is of paramount importance.

In this paper, we present several visible to thermal infrared multi- and hyperspectral remote sensing techniques for characterization of glacier debris which are applied to glacier energy balance, kinematic history and ice extent mapping. Glaciers in the Khumbu Himalayas will be used for testing the remote sensing techniques, with in situ field spectrometry and debris sample mineralogy and composition used as ground truth. To the authors' knowledge, no glaciologic study has explored full spectrum – visible to thermal infrared – data for qualitative and quantitative supraglacial debris characterization which is relevant to improving debris covered glacier mapping, understanding kinematic history as well as estimating thermal parameters of glaciers.

2 Optical remote sensing of glacier debris

In the following sections, we provide a review of optical satellite sensors used in this study and a brief background on spectral measurement of lithology.

2.1 Sensors

Earth observing satellite technology has advanced greatly in recent decades and allows for unprecedented spatial, temporal and spectral imaging of Earth's cryospheric surfaces, including difficult to access alpine and polar regions. Wavelength dependent spectral signatures can be used to identify surface material based on electromagnetic

reflection (0.4–3 μm) and emission (3–14 μm) (Goetz et al., 1983). Optical satellite instruments measure discrete spectral bands from the visible to the thermal infrared wavelengths (0.4–14 μm) and provide high resolution spectral information for determining surface materials (e.g.: snow, ice, rock, vegetation) at up to daily temporal resolutions and couple hundred meter spatial resolutions (e.g.: Medium Resolution Imaging Spectrometer Instrument, MERIS or Moderate Resolution Imaging Spectrometer, MODIS) or finer spatial resolutions of tens of meters and coarser temporal resolutions of more than ten days (e.g.: US/Japan Advanced Spaceborne Thermal Emission and Reflection Radiometer (ASTER) onboard the NASA Earth Observing System Terra satellite and US NASA/USGS Landsat mission satellites). Data from Landsat and ASTER are commonly used in glacier analysis, due to the finer spatial resolution (Hall et al., 1988; Paul et al., 2002; Andreassen et al., 2008) and will be among the sensors utilized in this study (Fig. 1).

The Landsat Earth observing satellite program began in 1972 (as Earth Resources Technology Satellite, ERTS) and has consisted of a several instruments over the past three decades: Landsat 1, 2, 3, 4 – Multispectral Scanner System (MSS), Landsat 4, 5 – Thematic Mapper (TM), and Landsat 7 – Enhanced Thematic Mapper Plus (ETM+). Landsat 7's ETM+ provides 16-day temporal resolution with 8 spectral bands: one panchromatic (pan) band at 15 m resolution, six visible to shortwave infrared bands at 30 m resolution, and one thermal band at approximately 60 m resolution. Unfortunately, the ETM+ scan line corrector (SLC) on the instrument failed in May 2003. ETM+ data post May 2003 exhibits wedge shaped gaps, resulting in a loss of approximately 22% of scene area (Storey et al., 2005). However, Landsat 7 ETM+ gap-filled data are available. Additionally, Landsat 5 TM, with similar spectral (7 bands) and spatial (30 m) resolution, continues to function at the date of this publication.

Launched onboard Terra in 1999, ASTER measures 14 optical bands at spatial resolutions from 15 to 90 m at 16-day temporal resolution. Specifically, ASTER offers three bands in the visible and near infrared (VNIR, 0.4–0.9 μm) at 15 m spatial resolution, six shortwave infrared bands (SWIR, 1.0–2.5 μm) at 30 m spatial resolution and

Optical remote sensing of debris covered glaciers

K. A. Casey et al.

Title Page

Abstract

Introduction

Conclusions

References

Tables

Figures

◀

▶

◀

▶

Back

Close

Full Screen / Esc

Printer-friendly Version

Interactive Discussion



Optical remote sensing of debris covered glaciers

K. A. Casey et al.

Title Page

Abstract

Introduction

Conclusions

References

Tables

Figures



Back

Close

Full Screen / Esc

Printer-friendly Version

Interactive Discussion



five thermal infrared bands (TIR, 3.0–12 μm) at 90 m spatial resolution. Intended particularly for spectral signature studies (Abrams, 2000), ASTER's spectral coverage in SWIR and TIR is unprecedented via satellite instrumentation. Unfortunately, after nine years of operation, in April 2008, the SWIR bands began to fail and are no longer suitable for geologic analysis. (To note, ASTER VNIR and TIR bands are still performing well at the date of this publication, SWIR data from 2000 to 2008 are usable.)

Part of a technological demonstration and validation mission, NASA's EO-1 satellite was launched in 2000 and operates in a sun-synchronous orbit on a 16-day repeat cycle (although images are not acquired continuously). EO-1 carries two pushbroom sensors: Hyperion and Advanced Land Imager (ALI). Hyperion uses a VNIR and a SWIR spectrometer to acquire 242 spectral bands from 0.4 to 2.5 μm (in 10 nm nominal increments) at 30 m spatial resolution. Of the 242 spectral bands, only 220 are calibrated due to low response of detectors in non-calibrated bands. Approximately 24 bands measure at the same wavelength between the VNIR and SWIR spectrometers. Thus, there are 196 distinct spectral bands – VNIR bands 8 through 57, and SWIR bands 77 through 224. Similar in spectral resolution to the Landsat series, ALI offers one pan band and 9 visible to shortwave infrared bands. Compared to Landsat TM and ETM+, ALI offers improved VNIR to SWIR spectral resolution at the same spatial resolution (30 m), and improved pan band spatial resolution (10 m vs. ETM+ pan 15 m). However, ALI offers no TIR spectral data. Although EO-1 was only planned to run for 2-years, operation has continued successfully and EO-1 is now managed by the United States Geological Survey (USGS) (all Hyperion and ALI instrument data after Beck et al., 2003).

2.2 Measuring lithology

The use of laboratory and field based spectroscopy in deriving mineral and chemical constituents began with pioneering investigations by McClure (1957, 1959); Lyon (1965); Hunt and Salisbury (1970a,b); Hunt et al. (1971a,b) as well as Clark and Lucey (1984) focusing strictly on ice/rock mixtures. Interpretation of reflectance and

emission spectra from optical satellite remote sensing for deriving mineral and chemical constituents has progressed over the past several decades (Vincent and Thomson, 1972; Goetz and Rowan, 1981; Clark et al., 1990; Hook et al., 1992; Rowan and Mars, 2003; Ninomiya, 2004). Laboratory and field based VNIR to SWIR and TIR spectral libraries serve as references for spectral analysis (Christensen et al., 2000; Baldrige et al., 2009) (Appendix A). Dominant anions, cations, trace constituents and crystal field structures strongly influence reflectance and emission spectra (Hunt, 1977; Gupta, 2003). Specifically, transition metal enrichment can be detected via use of VNIR (Rowan et al., 1986; Gupta, 2003; Rowan and Mars, 2003); hydroxide, sulfate and carbonate minerals can be analyzed using SWIR (Kruse, 1988; Rowan and Mars, 2003; Ninomiya et al., 2005); and silicate, carbonate, oxide, phosphate, and sulfate minerals via use of TIR (Gillespie et al., 1984; Hook et al., 1992; Gupta, 2003; Ninomiya et al., 2005). Traditionally, X-ray diffraction (XRD) can be used to semi-quantitatively identify mineralogy of in situ samples, while X-ray fluorescence spectrometry (XRF) can be used to provide a quantitative measurement of oxide compound weight percentage (e.g.: SiO_2 , Al_2O_3 , Fe_2O_3 , CaO) as well as trace element concentration (part per million, ppm) (e.g.: V, Co, Zn, Pb). In this paper, we utilize XRD and XRF analysis of glacier debris samples to qualitatively and quantitatively and investigate lithology (which we define as the description of rock composition and texture) via remote sensing data in light of glacier dynamics.

Previous hyperspectral and satellite multispectral geologic or geochemical remote sensing differentiation studies focus largely on arid terrain (e.g. Goetz et al., 1983; Sultan et al., 1987; Rowan et al., 2005). Spectral investigations of debris cover on glacier surfaces to date include: glacier extent mapping via Landsat thermal imaging (Lougeay, 1974, 1982), SPOT pan imagery and an applied artificial neural network (Bishop et al., 1999), Landsat TM and ASTER VNIR, TIR data mapping (Taschner and Ranzi, 2002), and combined VNIR, 1 SWIR band, TIR and geomorphic data (Shukla et al., 2010). Further morphometric glacier mapping approaches are presented in Paul et al. (2004) and Bolch et al. (2007). In addition to glacier extent studies, Shroder et al.

Optical remote sensing of debris covered glaciers

K. A. Casey et al.

Title Page

Abstract

Introduction

Conclusions

References

Tables

Figures

◀

▶

◀

▶

Back

Close

Full Screen / Esc

Printer-friendly Version

Interactive Discussion



(2000) inspected glacial debris cover via 4 SPOT VNIR bands to suggest mechanisms in which debris covered glaciers turn into rock glaciers; Wessels et al. (2002) used ASTER VNIR-TIR data to analyze spectral variability of supraglacial lakes in the Everest region; Suzuki et al. (2007) mapped thermal resistance of debris covered glaciers in the Lunana and Khumbu Himalayas, and Kääb (2005) utilized false color ASTER SWIR and TIR band composites to indicate debris patterns, source areas, and indication of flow regimes at Hispar glacier in the Karakorum, Pakistan and Unteraar glacier in the Grimsel region of the Swiss Alps. This study identifies VNIR-TIR multi- and hyperspectral satellite remote sensing methods for lithologic differentiation and characterization of supraglacial debris.

3 Study area

Fifteen percent of the Himalayan mountain range is covered by glaciers, constituting one of the largest areas of land-based ice outside of the Greenland and Antarctic ice sheets (Nesje and Dahl, 2000; Anthwal et al., 2006; Radic and Hock, 2010). We estimate glacier area in the Hindu Kush Himalayas to be around 65 000 km², and 8000 km² or roughly 15% of this glacier area is debris covered (unpublished initial Himalaya glacier inventory by the authors). Focusing on the Khumbu Himalaya study area (Fig. 2, 3), the Ngozumpa glacier is the longest glacier in Nepal at approximately 25 km (Benn et al., 2001) with Khumbu glacier measuring 17 km in length (Hambrey et al., 2008). The large size of these debris covered ablation areas provides ample spatial coverage to use remote sensing data (ranging from 15–90 m VNIR-TIR) in spectral debris cover analysis.

The climate in the region is strongly affected by the South Asian monsoon, mid-latitude westerlies, and El Niño Southern Oscillation (ENSO) (Benn and Owen, 2002). The Khumbu Himalayan glaciers experience summer precipitation that exceeds winter precipitation, allowing for simultaneously strong accumulation and ablation from late May through mid-September. Glaciologically referred to as summer accumulation type

Optical remote sensing of debris covered glaciers

K. A. Casey et al.

Title Page

Abstract

Introduction

Conclusions

References

Tables

Figures



Back

Close

Full Screen / Esc

Printer-friendly Version

Interactive Discussion



(Ageta and Higuchi, 1984; Benn and Owen, 1998), significant melt can occur in late fall and early winter months as was observed at Khumbu glacier in December 2009. The Ngozumpa and Khumbu glaciers are heavily debris covered due to frequent rock and ice avalanches from surrounding extreme topographic relief. High rates of supraglacial activity in terms of sediment transport, deposition, and glacial erosion (Benn and Owen, 2002) as well as the extreme topographic relief are characteristics that differentiate Himalayan glaciers from polar and other alpine glaciers.

Ngozumpa and Khumbu glacier surface debris consists primarily of leucogranite, greenschist and sillimanite gneiss dust, silts, sands, gravels, rocks and boulders, with primary mineral components including quartz, potassium feldspars (in the form of orthoclase and microcline), feldspars (albite, calcium-rich albite), micas (muscovite, biotite, phlogopite), and carbonates (calcite) (Pognante and Benna, 1993; Carosi et al., 1999; Searle, 1999; Searle et al., 2003). Extensive debris cover on both glacier tongues increases in depth down glacier and insulates the underlying ice (Kadota, 1997; Kadota et al., 2000; Byers, 2007; Hambrey et al., 2008). Both Ngozumpa and Khumbu glaciers are characterized by numerous supraglacial melt ponds (Wessels et al., 2002) and considerable relief of supraglacial debris with the height difference between peaks and troughs estimated at 20–50 m as observed during field work in 2009 and reported in Benn and Owen (2002). Downwasting or thinning of Khumbu Himalayan glaciers has been observed over the past several decades (Bolch et al., 2008a). In addition to downwasting, backwasting, or the ablation which occurs on exposed ice faces in debris covered areas, is a primary melt mechanism active on these glaciers. Backwasting was found to account for up to 20% of the total ablation of debris covered area by Nakawo et al. (1999). Backwasting related topographic inversion processes that occur on these debris-mantled glaciers, yield complex debris assemblages (detailed in Benn and Evans, 2010). Fushimi et al. (1980) field based maps of supraglacial debris types on the Khumbu glacier show a longitudinal band of schistic debris and lateral granitic debris bands, traced from the icefall to the terminus. These Khumbu glacier longitudinal supraglacial debris bands are reflective of surrounding

Optical remote sensing of debris covered glaciers

K. A. Casey et al.

Title Page

Abstract

Introduction

Conclusions

References

Tables

Figures



Back

Close

Full Screen / Esc

Printer-friendly Version

Interactive Discussion



lithology, and indicative of flow processes. Wave ogives occurring directly below the Khumbu icefall were noted by Hambrey et al. (2008), further suggesting glacial flow patterns also act as a control on the distribution of debris.

4 Data collection and methods

For this study, field work was conducted at the Ngozumpa and Khumbu glaciers in November and December 2009. Multiple glacier surface measurements were collected, including VNIR-SWIR field spectra, land surface temperature (LST), and physical samples of surface snow, ice, meltwater, and debris. Field measurements were conducted in the middle ablation area of the Ngozumpa glacier (approx 4735–4790 m a.s.l.) and in the upper ablation area of the Khumbu glacier (approx 5100–5285 m a.s.l.). Figure 3 and Table 1 detail the glaciers studied and in situ measurement locations.

4.1 Field spectrometry

Field spectra were measured using an Analytical Spectral Devices (ASD) FieldSpec Pro. The backpack portable laptop-driven FieldSpec Pro is comprised of three detectors that measure spectral reflectance from visible to shortwave infrared (0.35–2.5 μm). One VNIR 512-channel silicon photodiode detector operates along with two separately cooled, scanning, grated index SWIR indium gallium arsenide (InGaAs) photodiode detectors. Instrumental spectral resolution (full-width at half maximum) is 3 nm at 0.7 μm , 10 nm at 1.4 μm , and 12 nm at 2.1 μm , with spectral sampling steps of 1.4 nm from 0.35–1.05 μm and 2 nm from 1.05–2.5 μm (Analytical Spectral Devices, 2002). Field spectrometry reflectance measurement methods after Hall et al. (1992); Wiens et al. (2002) and Takeuchi and Li (2008) among others, were used in the field in order to allow for optimal comparison with satellite remote sensing data. More sophisticated field spectra measurement techniques (e.g. Sandmeier and Itten, 1999; Painter et al., 2003; Bourgeois et al., 2006) would have been desirable, however such equipment was not available nor logistically possible for use in this study.

Optical remote sensing of debris covered glaciers

K. A. Casey et al.

Title Page

Abstract

Introduction

Conclusions

References

Tables

Figures



Back

Close

Full Screen / Esc

Printer-friendly Version

Interactive Discussion



Optical remote sensing of debris covered glaciers

K. A. Casey et al.

Title Page

Abstract

Introduction

Conclusions

References

Tables

Figures



Back

Close

Full Screen / Esc

Printer-friendly Version

Interactive Discussion



Over 3360 spectra were collected from glacier snow, ice, debris, and vegetation categories at the Ngozumpa and Khumbu glaciers. Specifically, in excess of 1800 spectra were collected at the Ngozumpa glacier from 26–29 November 2009, while more than 1560 spectra were collected at the Khumbu glacier from 4–6 December 2009. Spectra were measured in ASD's raw mode on clear sky days within two hours of local solar noon (10:00 a.m.–2:00 p.m. LT). An 18° foreoptic and distances ranging from 10 cm to 1 m above the surface (relating to approximately 3 cm² to 30 cm² surface resolution, respectively) were used for spectral data acquisitions. A Spectralon calibration panel provided the reference reflectance material. For each targeted surface material, at least 20–30 ground based spectrometry measurements were collected in the nadir viewing direction. In situ sample sites were selected to cover a range of surface types, of both pure (e.g.: bare ice, snow, debris) and mixed targets (e.g.: snow and rock, ice and snow) – maximizing spectral acquisitions while maneuvering on the active debris covered glacier in the short solar noon temporal window. Spectral measurements were collected with the aim of assessing in situ reflectance measurements of both pure and mixed pixel spectral targets. Geographic location (GPS), surface temperature and physical samples were collected in conjunction with each set of spectral class measurements.

Determination of field spectrometry results involved converting instrumental raw mode digital numbers to spectral reflectance after Nicodemus et al. (1977). Measured target reflectance was divided by Spectralon calibrated reference surface reflectance, and multiplied by both calibration panel offsets and the user defined reflectance scale for each wavelength (0.35–2.5 μm). Due to FieldSpec Pro instrument variability from the 57 VNIR/SWIR individual optical fiber responses (MacArthur et al., 2007) as well as signal-to-noise ratios (Analytical Spectral Devices, 2002) and in order to compare field spectra with satellite spectral data, repeat field spectra over each target were averaged to form field spectral reflectance class signatures (here after referred to as spectral signatures).

4.2 Sample acquisition and analysis by X-ray diffraction and X-ray fluorescence spectrometry

In conjunction with spectral measurements, 19 samples of snow, ice, and melt water were collected in acid prepared 500 mL low density polypropylene Nalgene bottles, and 22 samples of supraglacial debris were collected in clean polyethylene bags (obtaining approximately 100 g of material per sample). All in situ samples were taken in duplicate and double polyethylene bagged. For this study, Ngozumpa and Khumbu glacier debris samples were analyzed for mineralogy and composition via powder XRD and XRF at the University of Oslo, Department of Geosciences (snow, ice and melt water results are presented in Casey et al., 2010). Debris samples were oven dried (2 days at 80 °C), crushed to a fine powder (less than 125 µm particle size) via a vibratory ringmill. Powder XRD was conducted via use of a Philips XPERT diffractometer (manufactured by PANalytical B.V., Almelo) with samples analyzed in FORCE Bulk Mode measuring from 2° to 65° 2Θ. Mineralogy was derived via use of PANalytical's X'pert Highscore software, with semi-quantitative peak area and weight factor estimates of percent composition were calculated after Moore (1997). For XRF, ten grams of oven dried fine powder was prepared into sample tablets and measured on a Philips PW2400 XRF spectrometer run via SuperQ Version 3 software in TRACES 7B mode. The following oxide compounds and trace elements were measured: SiO₂, Al₂O₃, Fe₂O₃, MgO, CaO, Na₂O, K₂O, and V, Co, Zn, Pb, Zr, Th, U. Accuracy of XRF results is 98%. XRD and XRF measurements along with field collected spectra and spectral library references provide an indication of Ngozumpa and Khumbu supraglacial debris mineralogy and composition.

4.3 Optical satellite data

To assess the potential of the unprecedented spectral data provided by current Earth observing sensors, satellite data from ALI, ASTER, Hyperion, and Landsat TM, ETM+ was used to investigate glacier debris cover in the Khumbu Himalayas. Spectral

TCD

5, 499–564, 2011

Optical remote sensing of debris covered glaciers

K. A. Casey et al.

Title Page

Abstract

Introduction

Conclusions

References

Tables

Figures

◀

▶

◀

▶

Back

Close

Full Screen / Esc

Printer-friendly Version

Interactive Discussion



Optical remote sensing of debris covered glaciers

K. A. Casey et al.

Title Page

Abstract

Introduction

Conclusions

References

Tables

Figures

◀

▶

◀

▶

Back

Close

Full Screen / Esc

Printer-friendly Version

Interactive Discussion



analysis methods for debris cover characterization included: hyperspectral reflectance, SWIR and TIR false color image composites, mineral abundance mapping via SWIR and TIR band indices and VNIR-TIR spectral angle relationships, TIR emissivity and land surface temperature (LST) mapping, and repeat image derived velocity and streamline estimations. The specific satellite data products used are as follows: Hyperion radiometrically corrected Level 1T data, Landsat TM Level 1T and ETM+ Level 1G radiometrically and geometrically corrected data, and the following ASTER products, Level 1B radiance-at-sensor data, Level 2 AST_07XT “Surface Reflectance VNIR & Crosstalk Corrected”, AST_05 “Surface Emissivity”, and AST_08 “Surface Kinetic Temperature”. A full discussion of EO-1 products is given in Beck (2003), Landsat products in Tucker et al. (2004) and Storey et al. (2005) and ASTER products in Abrams (2000) and Abrams et al. (2002). Satellite data acquisition dates, product names and methods used to investigate Khumbu Himalayan glacier debris cover are summarized in Table 2. Satellite remote sensing data were acquired with the closest temporal and seasonal (post-monsoon dry season) correlation in light of the previously mentioned instrument anomalies (Landsat ETM+ data prior to 2003 and ASTER SWIR data prior to 2008 are used).

For satellite reflectance analysis, digital numbers were converted to at-sensor radiance using sensor- and band-specific calibration settings (e.g.: gain, offset, solar irradiance). At-sensor radiance was converted to at-sensor (top-of-atmosphere) planetary reflectance for each band after Markham and Barker (1986) (Eq. 1).

$$\rho_p = \frac{(\pi \times L_\lambda \times d^2)}{(\text{ESUN}_\lambda \times \cos\theta_s)} \quad (1)$$

Where ρ_p is at-sensor planetary reflectance (unitless value from 0 to 100%),

L_λ is at-sensor radiance ($\text{m W cm}^{-2} \text{ sr}^{-1} \mu\text{m}^{-1}$),

d is the Earth-Sun distance (in Astronomical Units),

ESUN_λ is mean solar exoatmospheric irradiance ($\text{m W cm}^{-2} \mu\text{m}^{-1}$),

θ_s is solar zenith angle in degrees.

Planetary reflectance can vary from surface reflectance due to absorption of gases and/or scattering effects of aerosols and gases in the atmosphere (Tanre et al., 1990). For example, at-satellite reflectance was found to increase 5–17% after atmospheric corrections were applied to Landsat TM data at Forbindels glacier in Greenland (Hall et al., 1990). Atmospheric planetary to surface reflectance correction, especially over snow and ice, remains in development (Kaufman, 1989; Lu et al., 2002; Stamnes et al., 2004; Mars and Rowan, 2010). Thus, atmospheric corrections were restricted to those applied in validated products (i.e. AST_07XT) and in the Landsat derived LST (after Barsi et al., 2005). Planetary reflectance is presented with regard to Hyperion debris covered glacier analysis, however a brief overview of atmospheric correction options for use with hyperspectral satellite data are discussed in Sect. 5.3.1.

Horizontal surface displacements on the glaciers studied were derived using normalized cross-correlation between repeat Landsat TM near-infrared as well as repeat ETM+ pan data (Kääb and Vollmer, 2000; Debella-Gilo and Kääb, 2011). Relative surface ages were estimated from streamlines as interpolated from the horizontal surface displacement velocity fields (Haug et al., 2010). Such streamlines resemble real particle trajectories only under the assumption that a velocity field is constant over time.

5 Results

Khumbu Himalayan debris covered glacier field spectrometry, XRD and XRF debris sample analysis, and optical remote sensing methodology study results are presented in the following subsections.

5.1 Field spectrometry

This section provides an overview of the 3360 plus visible to shortwave infrared ice, snow, and debris spectral reflectance measurements collected at Ngozumpa and Khumbu glaciers. To begin, Fig. 4 displays spectral signatures acquired for Ngozumpa

Optical remote sensing of debris covered glaciers

K. A. Casey et al.

Title Page

Abstract

Introduction

Conclusions

References

Tables

Figures

◀

▶

◀

▶

Back

Close

Full Screen / Esc

Printer-friendly Version

Interactive Discussion



glacier fresh snow and Khumbu glacier bare ice in comparison with previous snow and ice reflectance measurements by Qunzhu et al. (1985); ASTER derived visible reflectance of bare ice for the Khumbu glacier measurement site is over plotted. Average standard deviation for Ngozumpa glacier fresh snow and Khumbu glacier bare ice spectral signatures is 0.011 and 0.002, respectively. Ngozumpa glacier snow and Khumbu glacier bare ice spectral signatures and ASTER derived spectral reflectance plot within documented reflectance variability (Qunzhu et al., 1985; Hall et al., 1990; Winther, 1993; Takeuchi, 2009). Reduction in the Ngozumpa glacier snow spectral signature, relative to the Qunzhu et al. (1985) fresh snow reflectance can be attributed to melt of several days; snow reflectance diminishes as snow grain size increases and melt progresses (O'Brien and Munis, 1975; Choudhury and Chang, 1979; Wiscombe and Warren, 1980; Warren, 1982; Dozier, 1989; Nolin and Dozier, 2000). Reduction in the Khumbu glacier bare ice spectral signature is attributed to ice pinnacles of roughly 2 to 10 m in height at the measurement location on the upper Khumbu glacier, beneath the icefall: spectra are lower in reflectance partially due to the mitigation of light caused by the ice pinnacle topography. Several snow and ice spectral signatures (clean snow, small particulate covered snow, gravel covered snow, half snow half ice "mixed pixel", and bare ice) collected in the upper Khumbu glacier are presented in Fig. 5. The half snow half ice "mixed pixel" spectral signature is roughly a linear mixture of the end-member clean snow and bare ice pure spectral signatures. Both fine particulates and gravel reduce visible reflectance of snow, with fine particulates displaying an absorption feature minima at approximately $0.5\ \mu\text{m}$, while larger scale gravel shows a more marked broad reduction in snow reflectance in the visible to near infrared, with absorption features beginning much earlier, at approximately $0.38\ \mu\text{m}$. A detailed investigation of all gravel on snow spectra suggested that absorption features similar to sillimanite gneiss ca. $0.35\text{--}1.0\ \mu\text{m}$ (reference spectrum seen in Appendix A) is resolved upon fine-scale spectral inspection.

Optical remote sensing of debris covered glaciers

K. A. Casey et al.

Title Page

Abstract

Introduction

Conclusions

References

Tables

Figures

◀

▶

◀

▶

Back

Close

Full Screen / Esc

Printer-friendly Version

Interactive Discussion



Optical remote sensing of debris covered glaciers

K. A. Casey et al.

Title Page

Abstract

Introduction

Conclusions

References

Tables

Figures



Back

Close

Full Screen / Esc

Printer-friendly Version

Interactive Discussion



Variability in snow optical reflectance can be attributed to a variety of components, including mineral composition of dust, soot, and organic material (Gajda, 1958; Warren and Wiscombe, 1980; Warren, 1982; Takeuchi et al., 2001). Snow carotenoid and chlorophyll absorption features at 0.55 and 0.68 μm , respectively, have been reported by Painter et al. (2001) and Takeuchi (2009). Absorption features near the chlorophyll absorption area were found in Khumbu snow spectra, however, fine debris was clearly visible in many of the snow samples and algal growth was not expected to dominate at the time of spectral measurements – though known to exist in the area (Yoshimura et al., 2000). Nevertheless, it is interesting to consider the factors affecting VNIR absorption, including metal cations within fine particulate debris or surface algal organisms and subsequent influence of these cations on spectral reflectance signatures (i.e. further investigation combining known metal cation absorption features (Appendix A) and XRD/XRF derived surface composition (Appendix B) with in situ and hyperspectral reflectance data).

Supraglacial debris field spectra were used to identify minerals present in Ngozumpa and Khumbu debris cover using spectral library references (Clark et al., 2007), with further validation provided by XRD analysis. Figure 6 presents an example of upper Ngozumpa glacier supraglacial debris mineral composition – a mixture of biotite, quartz and albite from field sample 3N (Table 3, Appendix B). This upper Ngozumpa glacier supraglacial debris spectra resulted in an approximately linear mixture of the three mineral components – biotite, quartz, and albite. Specifically, the slope of the biotite spectral library reference as well as the hydroxide related 1.4 μm OH bond absorption features from the quartz and albite reference spectra each are seen in the upper Ngozumpa debris mixture spectral signature. The standard deviation of the debris spectral signature was calculated at 0.013. Similar standard deviation magnitudes were found in the majority of spectral signatures – suggesting low variability within spectral measurements. To note, comparisons of debris spectral signatures with spectral library references should be regarded as qualitative – as spectral library reference spectra are from region specific, synthesized or altered materials, measured under

optimal or laboratory conditions with controlled factors that can impact spectral measurement (i.e.: illumination, temperature, pressure, humidity, wind) (Siegal and Abrams, 1976; Gupta, 2003).

Finally, the influence of melt water in fine particulate debris cover was observed in the supraglacial debris spectral signatures. The SWIR portion of the spectrum manifests characteristic water absorption features, which allow the amount of surface debris moisture to be estimated (Angstrom, 1925; Bowers and Hanks, 1965; Skidmore et al., 1975; Lobell and Asner, 2002). Ngozumpa supraglacial debris spectra presented in Fig. 7 of visually dry and wet mud display the subsequent variability in reflectance intensity. While general shapes of reflectance spectra are maintained, the amount of melt water determines the degree of reflectance intensity. Using reflectance moisture estimation (e.g. Bowers and Hanks, 1965; Liang, 2004; Zheng et al., 2005), water content was estimated at 5% and 15–20% from the two debris spectral signatures on the upper Ngozumpa glacier site. Spectral estimated supraglacial moisture content could be of key interest to glaciologic energy balance modelers, as debris moisture information is necessary for calculation of soil surface albedo (Liang, 2004). Improved supraglacial debris surface albedo could reduce errors in predictions of glacier ablation rates and mass loss.

5.2 X-ray diffraction and X-ray fluorescence measurements

Ngozumpa and Khumbu supraglacial debris rock, gravel, soil and silt mineralogy was determined by XRD to consist primarily of quartz, potassium feldspars (orthoclase and microcline), feldspars (albite, calcium albite), carbonates (calcite, ankerite, siderite), and micas (muscovite, phlogopite, biotite) (Table 3, Appendix B). These mineral classifications can be visualized in the reflectance and emission spectra of the dominant minerals (Appendix A) and will be further referred to in the optical remote sensing mineral mapping techniques discussed below (Sect. 5.3.3). Ngozumpa glacier samples were primarily quartz, feldspar – in the form of calcium albite, and mica – in the form of biotite, while Khumbu samples were primarily mica – in the form of muscovite, feldspar

Optical remote sensing of debris covered glaciers

K. A. Casey et al.

Title Page

Abstract

Introduction

Conclusions

References

Tables

Figures



Back

Close

Full Screen / Esc

Printer-friendly Version

Interactive Discussion



– in the form of calcium albite and quartz. XRD mineralogy results indicated minor percentages of calcite in 7 of the 8 Ngozumpa glacier samples, and 2 of the 14 Khumbu glacier samples, and trace amounts of chlorites in 2 of the 8 Ngozumpa glacier samples, and 9 of the 14 Khumbu glacier samples. XRD results from this study were found to be comparable with published data by Searle et al. (2003) among others detailed in (Sect. 3).

XRF oxide and trace element quantitative results provide validation for supraglacial debris reflectance characteristic investigation – as briefly covered in the previous section. XRF silica measurements are also compared with ASTER based silicate mapping results (Sect. 5.3.3). Primary mineral and XRF determined silica weight percent results are displayed in Table 3 and full XRF analytical results are given in Appendix B. These XRD/XRF supraglacial debris results provide quantitative data on the Khumbu and Ngozumpa glaciers not previously reported.

5.3 Optical satellite data

The ASTER Level 2 atmospherically and cross-talk corrected surface reflectance data product (AST_07XT) was utilized for comparison with in situ surface reflectance (subsequent satellite methods investigate planetary reflectance of glacier surfaces). An average of nearest satellite reflectance pixels to the in situ sample location – 4×4 pixels in visible bands, and 2×2 pixels in SWIR bands, corresponding to a spatial resolution of 60 m^2 – was chosen for comparison due to the temporal disparity between in situ acquired data and satellite derived data (6 years) and the velocity of the glaciers (roughly from 10–50 m per year) (Sect. 5.3.5). Although these temporal and spatial disparities are not ideal for comparisons (due to potential surface movement of studied lithology over time or in situ point to 60 m^2 spatial differences), a first-order assessment of lithologic characteristics and mapping is worthwhile, especially in this region with the thick debris cover and relatively low velocities. The ASTER spectral signature shape and absorption features match relatively well with the in situ spectral signatures, for example, shown in ice and debris comparisons (Figs. 4 and 6, respectively).

Optical remote sensing of debris covered glaciers

K. A. Casey et al.

Title Page

Abstract

Introduction

Conclusions

References

Tables

Figures



Back

Close

Full Screen / Esc

Printer-friendly Version

Interactive Discussion



CORrection Now (ACORN) and Fast Line-of-sight Atmospheric Analysis of Spectral Hypercubes (FLAASH) and are described in Gao et al. (2009). Hyperion-specific atmospheric correction approaches remain in discussion (e.g. Dadon et al., 2010; Wang et al., 2010). Unfortunately, commercial atmospheric correction software was not available to the authors, and simplified atmospheric correction methods – such as dark object subtraction – rescale entire band arrays, potentially masking valuable spectral information (Kääb, 2005; Ninomiya et al., 2005). Thus, Hyperion planetary reflectance supraglacial debris evaluation is qualitative in this study.

Without atmospheric correction, a few other methods in addition to qualitative reflectance can be used to analyze Hyperion data. For example, true and false color composites as well as at-sensor radiance indices can be utilized and are discussed below in Sects. 5.3.2 and 5.3.3, respectively. As a technological demonstration, Hyperion VNIR-SWIR spectral analysis of mineralogy and lithology proves promising (e.g. Griffin et al., 2005; Gleeson et al., 2010). Theoretically, Hyperion data used in conjunction with commercial spectral and atmospheric correction software could be successful in discriminating small-scale wavelength and absorption depth-dependent characteristics of supraglacial debris (e.g. using continuum removal techniques (Clark and Lucey, 1984) to determine debris components and concentrations).

5.3.2 Shortwave and thermal false color composites

As suggested in the above hyperspectral remote sensing section, false color image composites highlight components not evident in true color images (e.g., Fig. 3). In addition to the VNIR-SWIR spectral resolution provided by ALI and Hyperion sensors, Landsat and ASTER offer thermal spectral bands (Fig. 1) that can be used to identify and classify glacier debris cover (Kääb, 2005). Landsat ETM+ thermal band 6 (11 μm) allows for spectral emission analysis of carbonate and silicate content in supraglacial debris, and Landsat ETM+ SWIR bands 5 and 7 (1.65 and 2.2 μm , respectively) indicate hydroxyl content, common to clays and hydrated silicates (see Appendix A for spectral features). Figure 9 displays a Landsat ETM+ SWIR band 5, 7 and TIR band

Optical remote sensing of debris covered glaciers

K. A. Casey et al.

Title Page

Abstract

Introduction

Conclusions

References

Tables

Figures



Back

Close

Full Screen / Esc

Printer-friendly Version

Interactive Discussion



6 false color (red, green, blue – RGB) image composite from 24 January 2003 of Ngozumpa and Khumbu field study sites as well as regional glaciers. Supraglacial debris composition variability is displayed by the coloring – yellow indicates silica-rich granites, while blue highlights carbonate-rich gneiss. For example, the Khumbu glacier longitudinal schistic supraglacial debris band starting from the icefall down the center of the glacier reported by Fushimi et al. (1980) can be visualized in blue in the Fig. 9 false color composite, with lateral granite debris bands visualized in yellow. Similar carbonate-rich vs. silica-rich longitudinal supraglacial debris bands are visible on upper Ngozumpa glacier.

False color SWIR/TIR composites quickly visualize supraglacial mineral variability. Although similar total SiO₂ content was found at all six Ngozumpa and Khumbu in situ samples sites (Appendix B and Table 3), the more uniform spatial distribution of silicates on Ngozumpa glacier can be easily differentiated from the more distinct silicate-rich vs. carbonate-rich mineral classes found on the Khumbu glacier using the SWIR/TIR false color composite technique. Further, false color composites can provide an indication of mass flux. In Fig. 9, a suggestion of limited mass flux transferred to at glacier confluences can be seen at the Khangri Shar, Khangri Nup and Khumbu glacier confluence as well as the Gyubanare, Ngozumpa glacier confluence by the distinct shifts in supraglacial mineralogy.

5.3.3 Mineralogic mapping

The rich SWIR and TIR spectral resolution provided by ASTER allow for qualitative and quantitative approaches to mapping surface mineralogy. Three such approaches are presented in this section. First, SWIR and TIR based mineralogic indices are evaluated using ASTER at-sensor radiance data. Second, TIR emissivity silica weight percent mapping is presented. Third, the Spectral Angle Mapper (SAM) algorithm after Kruse et al. (1993), is discussed for semi-automated identification of supraglacial components. The three types of mineral mapping provide different advantages and limitations in characterizing supraglacial lithology. Of the methods, SAM is unique in the

Optical remote sensing of debris covered glaciers

K. A. Casey et al.

Title Page

Abstract

Introduction

Conclusions

References

Tables

Figures



Back

Close

Full Screen / Esc

Printer-friendly Version

Interactive Discussion



potential to use discrete bands from the full VNIR-TIR spectrum, while TIR emissivity silica weight percent and mineral indices offer more quantitative estimates of specific mineral abundances.

SWIR Indices

5 SWIR mineral indices use wavelength dependant spectral absorption features to estimate mineral abundance. Several mineral indices are available and were evaluated (e.g. Vincent and Thomson, 1972; Ninomiya, 2003, 2004; Ninomiya et al., 2005). Based on the dominant minerals in the Khumbu Himalaya study area, the layered silicate index (LS) (Eq. 2) and calcite index (CA) (Eq. 3) after Ninomiya (2003) are
10 presented in this study.

$$LS = \frac{(AST4 \times AST8)}{(AST5 \times AST6)} \quad (2)$$

$$CA = \frac{(AST6 \times AST9)}{(AST8^2)} \quad (3)$$

Where $ASTn$ corresponds to ASTER spectral band number n .

15 The LS and CA SWIR indices target bands that measure hydroxyl ($2.2 \mu\text{m}$) and carbonate ($2.35 \mu\text{m}$) absorption features, respectively (See Appendix A). At-sensor radiance band ratios reduce atmospheric and topographic influences (including illumination variability) (Abrams et al., 1983; Mather, 1987; Käab, 2005), highlight information not evident in single band or three-band true or false color composite images, and provide a quantitative estimate of mineral abundances. Layered silicate mineral abundance at
20 Ngozumpa and Khumbu glaciers calculated from (Eq. 2), ASTER L1B at-sensor radiance data from 29 November 2005 is shown in Fig. 10. SWIR mineral index values can be further applied as thresholds in algorithms or in creation of thematic mineral abundance maps. For the scope of this study a grayscale image with darker shades indicating lower amounts of silicates and brighter shades indicate higher amounts of

Optical remote sensing of debris covered glaciers

K. A. Casey et al.

Title Page

Abstract

Introduction

Conclusions

References

Tables

Figures



Back

Close

Full Screen / Esc

Printer-friendly Version

Interactive Discussion



silicates is presented. This grayscale silicate index map can also be used to quickly visualize kinematic flow, similar to that reported in Sect. 5.3.2. However, in addition to visualization, the SWIR LS and CA indices offer quantifiable mineral-specific abundances.

5 TIR Indices

Thermal at-sensor radiance indices after Ninomiya et al. (2005), offer the first strictly thermal spectrum based technique presented in this study. The thermal portion of the spectrum is described as the most important region of the spectrum for differentiating geology of terrestrial materials (Gupta, 2003). However, satellite spatial resolution in the thermal bands is considerably lower than VNIR or SWIR (e.g. in ASTER VNIR 15 m, SWIR 30 m, TIR 90 m spatial resolution). Nevertheless, TIR indices are utilized to study the abundance of the following minerals (and mineral groups) in the study region glacier debris cover: quartz, silicate, and carbonate. Rocks containing these mineral groups express characteristic emission features in the thermal infrared (see also Appendix A). TIR based band ratios to estimate carbonate, quartz and silica containing lithology are presented in Eqs. (4–6) (Ninomiya et al., 2005).

$$CI = \frac{(AST13)}{(AST14)} \quad (4)$$

$$QI = \frac{(AST11^2)}{(AST10 \times AST12)} \quad (5)$$

$$MI = \frac{(AST12 \times AST14^3)}{(AST13^4)} \quad (6)$$

20 Where $ASTn$ corresponds to ASTER spectral band number n .

The carbonate index (CI) is utilized to detect the primary carbonate minerals calcite and dolomite – with high values of CI indicating presence of these minerals (absorption features at 11.4 μm for calcite, 11.2 μm for dolomite). Further, pure carbonate will

Optical remote sensing of debris covered glaciers

K. A. Casey et al.

Title Page

Abstract

Introduction

Conclusions

References

Tables

Figures



Back

Close

Full Screen / Esc

Printer-friendly Version

Interactive Discussion



provide a high CI value in conjunction with and low QI and MI values. The quartz index (QI) not only is indicative of quartz, but also low QI values signal potassium feldspar and gypsum. The mafic index (MI) correlates with silicate content, and is also sensitive to carbonate content in rocks. A simple silicate index ratio of band 12 to band 13 can be used – but for the differentiation from carbonates, Eq. (6) is used. A MI value greater than 0.90 corresponds to mafic rocks, while a MI value greater than 0.92 corresponds to ultramafic rocks (Ninomiya et al., 2005). To note, Ninomiya et al. (2005) concluded the stability of TIR mineral indices irrespective of surface temperature, elevation and atmospheric condition.

TIR emissivity to map silica abundance

Another technique to extract the dense geologic information available in the thermal bands is emissivity derived silica abundance mapping. Satellite emissivity weight percent of silica (SiO₂) after (Hook et al., 1992; Miyatake, 2000; Watanabe and Matsuo, 2003) is evaluated on Khumbu Himalaya supraglacial debris. Equation (7) (after Watanabe and Matsuo, 2003) displays the SiO₂ weight percent from emissivity values of ASTER TIR bands 10, 11, 12, and 13.

$$\text{SiO}_2 = 56.20 - 271.09 \times \log \left[\frac{(\text{ASTe10} + \text{ASTe11} + \text{ASTe12})}{(3 \times \text{ASTe13})} \right] \quad (7)$$

Where ASTe n corresponds to ASTER AST_05 surface emissivity product band number n .

Using the ASTER Surface Emissivity AST_05 product, silica weight percent abundance was derived for the Khumbu Himalaya region glaciers (Fig. 11). The ASTER derived silica weight percent estimates were compared with in situ XRF determined SiO₂ weight percent, with general agreement in consideration of the spatial resolution variation from in situ to 90 m² (ASTER TIR resolution) as well as the temporal resolution discrepancy of approximately 6 years (Table 3). Specifically, the difference between the XRF derived silica weight percent and TIR emissivity calculated silica weight percent

Optical remote sensing of debris covered glaciers

K. A. Casey et al.

Title Page

Abstract

Introduction

Conclusions

References

Tables

Figures

◀

▶

◀

▶

Back

Close

Full Screen / Esc

Printer-friendly Version

Interactive Discussion



of the Ngozumpa and Khumbu glacier field measurement sites ranged from a 4.0 to 15.1 percent difference. This technique has been found to allow quantitative estimates of silica content from daytime TIR acquisitions (Hook et al., 2005). Further, mapping of silica content in supraglacial debris covered glacier areas may potentially provide a first order look at glacial activity, sediment transport, weathering processes, glacial erosion or areas prone to differential melt based on differing supraglacial debris composition. Further, in the Khumbu Himalaya test region, the silica percent thematic map outlined debris covered ice extent.

Spectral angle mapper

Finally, the spectral angle mapper (SAM) algorithm provides a powerful means to classify surface materials. The SAM classification algorithm evaluates general shape and angles user input spectral data to assign thematic mineral and non-mineral classes (Kruse et al., 1993). SAM is suggested by Dematte et al. (2004) and Chen et al. (2007) as the optimal method for classifying surface lithology due to the integration of VNIR, SWIR and TIR data for spectral signature identification. Chen et al. (2007), found SAM to particularly outperform other minimum-distance classification and spectral feature fitting when analyzing silicates, carbonates and other minerals expressing TIR absorption over arid terrain. SAM was evaluated in this study (using ASTER L1B data) and preliminary SAM analysis on Khumbu glacier provided successful first-order differentiation of bare ice, snow, silica, calcite, and vegetation land cover. In comparison to the previously mentioned lithologic mapping methods, an advantage of SAM is the ability to map not only mineralogy, but also other land cover types, including snow, ice, and vegetation within the same classification and without requiring a full hyperspectral data set. Further, sensitivity to illumination and albedo data acquisition effects are addressed by the SAM algorithm design.

Optical remote sensing of debris covered glaciers

K. A. Casey et al.

Title Page

Abstract

Introduction

Conclusions

References

Tables

Figures



Back

Close

Full Screen / Esc

Printer-friendly Version

Interactive Discussion



5.3.4 Land surface temperature

Another thermal spectral band based glacier surface mapping technique is calculation of land surface temperature (LST) on glaciers. Thermal band derived LST was evaluated from the ASTER AST_08 Land Surface Temperature product, as well as from calculated Landsat the ETM+ and TM thermal band (after Barsi et al., 2005; explained in Hall et al., 2008) over Ngozumpa and Khumbu glaciers. Due to the nearly temporal coincidence of Landsat TM (31 October 2009) and in situ LST measurements (November, December 2009), Landsat TM data was utilized for satellite derived glacier debris cover LST analysis. Figure 12 shows Landsat TM calculated LST on Khumbu glacier, and Fig. 13 for Ngozumpa glacier. A longitudinal LST transect from the Khumbu icefall approximately 2 km down glacier displays a 15 °C increase in temperature. A similar Khumbu glacier LST trend is reported in Nakawo et al. (1999), and in Hall et al. (1987) using Landsat TM calculated LST.

In situ glacier surface temperatures measured in November and December 2009 field work sites were compared with the Landsat TM 31 October 2009 derived surface temperatures. In situ temperatures measured of snow, ice, and debris were averaged at each of the three Ngozumpa and three Khumbu glacier measurement locations. For example, in situ temperatures of 0.4 °C for upper Khumbu, 2.4 °C for mid-Khumbu, and 6.7 °C for lower Khumbu sample sites relate to Landsat TM 120 m pixel resolution LST's of -3.2, 4.8, 3.4 °C, respectively. In consideration of the spatial and temporal resolution disparities (satellite acquisition time 10 a.m. with some areas in shadows vs. in situ measurement disparity 2 h about solar noon, also point to 120 m² spatial disparity), general agreement was found between temperature measurements.

Used in conjunction with LST, other optical remote sensing supraglacial characterization methods may improve input toward glaciologic energy balance models. For example, LST and debris composition, could be analyzed to estimate differential solar absorption and subsequent impacts to ice melt rates (e.g.: Ngozumpa glacier measured gneiss surface temperature 24.1 °C vs. granitic debris 11.0 °C, and as shown in calcite index (Eq. 3), LST across Ngozumpa glacier transect Fig. 13).

Optical remote sensing of debris covered glaciers

K. A. Casey et al.

Title Page

Abstract

Introduction

Conclusions

References

Tables

Figures



Back

Close

Full Screen / Esc

Printer-friendly Version

Interactive Discussion



5.3.5 Glacier velocity, streamlines

Repeat optical Landsat images were used to derive glacier velocities at Ngozumpa and Khumbu glaciers. Specifically, normalized cross-correlation between Landsat ETM+ orthorectified 15 m pan data from 30 October 2000 and 4 October 2002 was used to derive a velocity displacement field. Velocity measurement errors were detected and filtered using a threshold on the correlation coefficient. Some remaining spurious vectors were removed manually. To ensure that the glacier surface velocities did not change significantly between 2000–2002 and the time of our in situ sampling, displacements were also derived from 30 m spatial resolution near-infrared band Landsat TM data from 5 November 2005 and 31 October 2009. No significant temporal changes were found. Optical feature tracking based velocity of both the Ngozumpa and Khumbu glaciers is estimated at 60 m/yr in the upper ablation zones to less than 5 m/yr in the lower ablation zones with errors estimated to be approximately 8–15 m for the ETM+ pan derived displacements (0.5–1 pixel; i.e. 4–7 m/yr) (Fig. 14). Glacier velocity rates estimated in this study are comparable to Khumbu Himalayan glacier velocity rates derived from synthetic aperture radar (SAR) feature tracking (Luckman et al., 2007; Hambrey et al., 2008; Quincey et al., 2009) as well as optical imagery (SPOT – Seko et al., 1998; Ikonos and ASTER – Bolch et al., 2008b; and COSI-Corr (Co-registration of Optically Sensed Images and Correlation, from Leprince et al., 2007) derived ASTER – Scherler et al., 2008). (Note, Quincey et al. (2009) derived Ngozumpa glacier velocity, while all other listed references refer to Khumbu glacier velocity studies.)

Further, theoretical supraglacial particulate streamlines on Ngozumpa and Khumbu glaciers were calculated and indicate time scales of 380 and 450 years, respectively (Fig. 14). Streamline interpolation stops at locations on glacier when velocities decrease below the margin of error – around 4 m/yr. Thus, 380 year Ngozumpa and 450 year Khumbu glacier streamline estimations represent minimum glacier ablation area ages. The Khumbu glacier streamline estimate from this study corresponds well with the Fushimi (1978) in situ, structural-derived estimate of Khumbu glacier ice at 410 ± 110 years.

Optical remote sensing of debris covered glaciers

K. A. Casey et al.

Title Page

Abstract

Introduction

Conclusions

References

Tables

Figures



Back

Close

Full Screen / Esc

Printer-friendly Version

Interactive Discussion



Optical remote sensing of debris covered glaciers

K. A. Casey et al.

Title Page

Abstract

Introduction

Conclusions

References

Tables

Figures

◀

▶

◀

▶

Back

Close

Full Screen / Esc

Printer-friendly Version

Interactive Discussion



The glacier ablation area velocity rates, directional flow vectors, as well as streamline estimations provide a “time scale” of the glacier ablation zone. Use of optical satellite remote sensing velocity and streamline approximations provide a powerful tool to use in conjunction with the previously discussed lithologic mapping techniques. For example, streamline dating could be utilized to give a crude, first-order approximation of “debris age” by supraglacial debris type. First-order streamlines, used with robust glaciologic sediment dating studies, such as Benn and Owen (2002); Owen et al. (2009), could roughly estimate glacier sediments dates of regional glaciers lacking field studies.

Velocity vectors indicate debris transport paths which can be compared to debris source and glacial transport paths observed from multi- and hyperspectral derived lithologic differences. Difference between current velocity fields and cumulative transport paths derived from lithology suggests a change of glacial mass movement over time, for example, represented by surges and looped moraines. Further, velocities and streamlines together with supraglacial lithologic information can improve estimations of expected weathering and diagenesis of debris.

6 Synthesis

From the several methods explored in this study, some of the most significant synergistic applications include, spectral based supraglacial component identification, description of mass flux, indication toward weathering and activity, estimation of thermal parameters, as well as mapping of debris covered ice extent.

Use of in situ VNIR-SWIR spectral signatures allow for identification of supraglacial components, for example of Khumbu snow and ice types (Fig. 5) or Ngozumpa supraglacial debris variability and moisture content (Figs. 6 and 7). Supraglacial mineral compositions can be used to indicate sources of lithology and subsequent diagenesis. Satellite spectral reflectance – Hyperion and ALI with 196 and 9 VNIR to SWIR spectral bands, respectively, and ASTER and Landsat with 14 and 7 VNIR to TIR spectral bands, respectively – provide potential to identify supraglacial components by spectral signatures (e.g., Hyperion qualitative planetary reflectance Sect. 5.3.1,

Fig. 8, SAM algorithm Sect. 5.3.3). Differentiation of glacier debris can allow for analysis of glacier debris sources and multidimensional debris transport paths (Figs. 9 and 10). Further, mineral indices and emissivity can also be used for identification or relative abundances of minerals in supraglacial debris, such as calcite abundance on Ngozumpa glacier (Eq. 3, Fig. 13) or Khumbu Himalaya regional silicate supraglacial abundance (Figs. 10 and 11). Synergistic inspection of supraglacial debris variability can bridge the gap in detecting debris sources and using identified components to describe glaciologic parameters such as supra- or englacial glacial transport routes.

A second important combined application of the optical remote sensing methods is in describing glacier mass flux. False color composites visually allow for speculation of mass flux; in conjunction with repeat imagery velocity and supraglacial particulate flow estimations, a more quantitative estimate of mass transport can be made. For example, Fig. 9 visually indicates limited to negligible transport of mass from Khangri Shar and Khangri Nup glaciers at the convergence with Khumbu glacier by the distinct visual supraglacial debris types. Repeat optical image matching velocity and streamlines (Fig. 14) further give low velocities and flow from Khangri Shar and Khangri Nup glaciers into the Khumbu glacier. This limited mass flux can also be seen in such a false color composite, velocity comparison at Gyubanare glacier confluence with Ngozumpa glacier (Figs. 9 and 14). Streamlines provide a first-order assessment of supraglacial movement (Sect. 5.3.5). Further, input of material to glacier surfaces, such as from a rock avalanche of distinct lithology, can be detected and characterized with false color composites. This supraglacial mass flux analysis is describes not only present day, but also years and decades past due to the debris patterns archived in the supraglacial debris.

Description of supraglacial activity and weathering processes is a third important synergistic application of the optical remote sensing debris characterization methods. Emissivity percent silica mapping may provide information on glacier activity rates and diagenesis (Fig. 11). In the Khumbu Himalaya test region, a silica percent thematic map provided indication of debris covered ice extent, and compared with repeat image

Optical remote sensing of debris covered glaciers

K. A. Casey et al.

Title Page

Abstract

Introduction

Conclusions

References

Tables

Figures

◀

▶

◀

▶

Back

Close

Full Screen / Esc

Printer-friendly Version

Interactive Discussion



velocity estimations, areas of higher velocities had correspondingly high silica composition. Supraglacial activity can also be indicated by the SWIR and TIR mineral indices – Fig. 10 suggests glacier kinematic pulses have occurred on the upper Ngozumpa glacier. Furthermore, the type of the material can be pinpointed by hyperspectral reflectance signature data – potentially confirming pre-weathered (or higher silica content) supraglacial debris material, for example in the upper ablation zone, and more heavily weathered (lower silica content) supraglacial debris in the lower ablation zone.

A fourth area of importance to glaciologic remote sensing is describing thermal supraglacial characteristics. Surface temperature can be calculated from sensors which acquire thermal data. In this study Landsat and ASTER surface temperature data was evaluated at Khumbu and Ngozumpa glaciers (Figs. 12 and 13). Glacier surface temperature was found to vary depending on the amount of debris cover as well as the composition of the debris and position on glacier. Temperature in conjunction with debris moisture content estimates (Fig. 7), hyperspectral mineral differentiation (Fig. 8), and/or mineral abundances (Fig. 10), more accurately describes surface parameters and could be crucial to reducing errors in satellite derived ablation rates and processes. Even further synergy of thermal and velocity data could be used to investigate climate interaction with debris covered ice, and to assess stagnation of flow toward the glacier terminus, the formation of supraglacial meltwater and subsequent glacial disintegration. Such glacier debris pattern analysis could reveal low magnitude, high repeat frequency mass events vs. episodic pattern high magnitude event, low frequency mass events. Spectral reflectance of debris covered ice can provide insight toward differential surface radiative absorption.

Finally, mapping of debris covered ice remains a challenge for optical remote sensing. Combination of methods presented in this study, for example the silica thematic mapping (Fig. 11), false color SWIR/TIR composites (Fig. 9), surface temperature (Figs. 12 and 13), and velocity (Fig. 14) methods all provide estimations of debris covered ice extent. Use of these techniques over debris covered ice area may be useful in improving debris covered glacier mapping.

Optical remote sensing of debris covered glaciers

K. A. Casey et al.

[Title Page](#)[Abstract](#)[Introduction](#)[Conclusions](#)[References](#)[Tables](#)[Figures](#)[⏪](#)[⏩](#)[◀](#)[▶](#)[Back](#)[Close](#)[Full Screen / Esc](#)[Printer-friendly Version](#)[Interactive Discussion](#)

7 Conclusions

Debris often covers a moderate to significant portion of glacier ablation areas. We estimate debris to cover approximately 15% of Hindu Kush Himalaya glaciers, relating to 8000 km² of debris covered ice. The presence and extent of supraglacial debris impacts radiative and surface processes of glaciers, and characterization of this debris can be used to indicate sources, paths and magnitudes of glacial transport as well as energy balance related glaciologic variables.

This study identified significant variability in the debris cover in the Khumbu Himalayan region glaciers. In situ hyperspectral imaging and XRD/XRF geochemical analysis was used to identify minerals, mineral mixtures, and moisture content of Ngozumpa and Khumbu glacier debris. Satellite planetary reflectance hyperspectral imaging was used to qualitatively differentiate surface components on Imja, Lhotse Shar, Gyubanare and Khangri Nup glaciers. We mapped supraglacial debris silica and calcite mineral abundances quantitatively with SWIR and TIR mineral indices, and silica weight percent quantitatively with TIR emissivity mapping across Khumbu Himalaya regional glaciers. Qualitatively, supraglacial mineral variability of Khumbu Himalayan glacier debris was mapped with false color SWIR/TIR image composites and differentiated silica-rich granite debris from carbonate-rich gneiss debris. Using false color image composites, mineral indices and repeat image derived velocity data, reduced glacial confluence mass flux of Gyubanare into Ngozumpa and Khangri Nup to Khumbu was determined. Similarly, the SWIR silica mineral index highlighted distinct kinematic pulses on the upper Ngozumpa glacier. Supraglacial temperatures were compared with calcite supraglacial debris abundance across Ngozumpa glacier and increased calcite supraglacial composition was found to correlate with increased supraglacial temperatures.

Synergistic application of the optical remote sensing supraglacial characterization methods presented are relevant to debris covered glaciers on a global scale in improving glaciologic interpretations of thermal, mass flux and debris covered ice extent.

Optical remote sensing of debris covered glaciers

K. A. Casey et al.

Title Page

Abstract

Introduction

Conclusions

References

Tables

Figures



Back

Close

Full Screen / Esc

Printer-friendly Version

Interactive Discussion



Optical remote sensing of debris covered glaciers

K. A. Casey et al.

Title Page

Abstract

Introduction

Conclusions

References

Tables

Figures



Back

Close

Full Screen / Esc

Printer-friendly Version

Interactive Discussion



Tuning the methods to the lithology of the region, debris covered glacier extent mapping may be delineated with combined use of false color composites, silica thematic mapping or region-specific mineral abundances, velocity fields and supraglacial temperature. Key methods applicable to thermal parameters include debris moisture estimations and use of mineral abundances to investigate supraglacial temperature variability. Kinematic processes are highlighted by combination of false color composites and mineral indices with velocity displacement fields and streamlines. Further, techniques can even be used to bridge the gap between field measurements and satellite based glacier estimations (e.g. with regard to improving glacier melt modeling).

Crucial to application of these methods in debris covered glacier monitoring is satellite sensor longevity and future sensors availability. As previously noted, some satellite instruments used in this study are no longer functioning optimally (Landsat ETM+ SLC gaps post 2003, ASTER SWIR failure post 2008). Landsat TM (and ETM+ gap-filled), ASTER VNIR and TIR as well as EO-1 ALI and Hyperion sensors offer current freely available spectral data sources. Forthcoming NASA optical satellite remote sensing missions include the National Polar-orbiting Operational Environmental Satellite System Preparatory Project (NPP) and National Polar-orbiting Operational Environmental Satellite System (NPOESS). ESA's Sentinel satellites with optical sensors aimed at collecting 10 m spatial resolution and 5 day temporal resolution prove extremely promising for glacier studies. Airborne hyperspectral sensors may be important tools to utilize during spaceborne instrumentation gaps.

High spectral and spatial resolution optical remote sensing is paramount for glacier monitoring. The wealth of current spectral satellite data has the potential to be used more broadly in supraglacial debris variability assessment. Improved satellite glacier debris cover characterization will lead to reduction of uncertainties in glacier extent mapping, glaciologic thermal parameters as well as glacial kinematic history and flow estimations, ultimately potentially advancing our understanding of debris covered ice ablation and mass loss.

Acknowledgements. This work was funded by the Department of Geosciences at the University of Oslo, Norway and European Space Agency's GlobGlacier project aimed at establishing protocols to map the world's glaciers via satellite remote sensing observations (Loan 585.1210 to DIB). We thank Alasdair MacArthur and Chris MacLellan of the Natural Environment Research Council Field Spectroscopy Facility for assistance with the field spectrometer loan. We also thank University of Oslo Department of Geosciences personnel Ruikai Xie and Berit Løken Berg as well as Misganu Debella-Gilo for assistance with XRD/XRF and velocity analysis, respectively. Thanks to Geir Moholdt for reviewing an earlier version of the manuscript. A special acknowledgement is due to Nima Sampang Rai for his help during field work in Nepal, as well as Rajesh Thapa and Samjwal Bajracharya at the International Centre for Integrated Mountain Development *ICIMOD* for logistic support in Kathmandu, Nepal.

References

- Abrams, M. J.: The advanced spaceborne thermal emission and reflection radiometer (ASTER): data products for the high spatial resolution imager on NASA's Terra platform, *Int. J. Remote Sens.*, 21(5), 847–859, 2000. 504, 511
- Abrams, M. J., Brown, D., Lepley, L., and Sadowski, R.: Remote sensing for porphyry copper deposits in Southern Arizona, *Econ. Geol.*, 78, 591–604, 1983. 520
- Abrams, M. J., Hook, S. J., and Ramachandran, B.: ASTER user handbook, available at: http://asterweb.jpl.nasa.gov/content/03_data/04_documents/aster_user_guide_v2.pdf, last access: 4 August 2010, 2002. 511
- Adhikary, S., Nakawo, M., and Seko, K.: Dust influence on the melting process of glacier ice: experimental results from Lirung Glacier, Nepal Himalayas, *Chapt. Debris-Covered Glaciers*, IAHS, Oxfordshire, UK, 43–52, 264, 2000. 501
- Ageta, Y. and Higuchi, K.: Estimation of mass balance components of a summer-accumulation type glacier in the Nepal Himalaya, *Geogr. Ann. A*, 66, 249–255, 1984. 507
- Analytical Spectral Devices, I.: *FieldSpec Pro User's Guide*, available at: <http://support.asdi.com/Document/Viewer.aspx?id=19>, last access: 5 October 2010, 2002. 508, 509
- Andreassen, L. M., Paul, F., Kääb, A., and Hausberg, J. E.: Landsat-derived glacier inventory for Jotunheimen, Norway, and deduced glacier changes since the 1930s, *The Cryosphere*, 2, 131–145, doi:10.5194/tc-2-131-2008, 2008. 503

Optical remote sensing of debris covered glaciers

K. A. Casey et al.

Title Page

Abstract

Introduction

Conclusions

References

Tables

Figures



Back

Close

Full Screen / Esc

Printer-friendly Version

Interactive Discussion



Optical remote sensing of debris covered glaciersK. A. Casey et al.

[Title Page](#)[Abstract](#)[Introduction](#)[Conclusions](#)[References](#)[Tables](#)[Figures](#)[◀](#)[▶](#)[◀](#)[▶](#)[Back](#)[Close](#)[Full Screen / Esc](#)[Printer-friendly Version](#)[Interactive Discussion](#)

- Angstrom, A.: The albedo of various surfaces of the ground, *Geogr. Ann.*, 7, 323–342, 1925. 515
- Anthwal, A., Joshi, V., Sharma, A., and Anthwal, S.: Retreat of Himalayan glaciers – indicators of climate change, *Nat. Sci.*, 4(4), 53–59, 2006. 506
- 5 Atwood, D., Meyer, F., and Arendt, A.: Using L-band SAR coherence to delineate glacier extent, *Can. J. Remote Sens.*, 36, S186–S195, 2010. 501
- Baldrige, A., Hook, S., Grove, C., and Rivera, G.: The ASTER spectral library version 2.0, *Remote Sens. Environ.*, 113, 711–715, 2009. 505
- Barsi, J. A., Schott, J. R., Palluconi, F. D., and Hook, S. J.: Validation of a web-based atmospheric correction tool for single thermal band instruments, vol. 5882, *Proceedings of SPIE*, SPIE, Bellingham, Washington, USA, 2005. 512, 524
- 10 Beck, R.: EO-1 User Guide v.2.3, available at: <http://edcns17.cr.usgs.gov/eo1/documents/EO1userguidev2pt320030715UC.pdf>, last access: 18 October 2010, 2003. 511
- Benn, D. I. and Evans, D. J.: *Glaciers and Glaciation*, Hodder Education, London, 2010. 501, 507
- 15 Benn, D. I. and Owen, L. A.: The role of the indian summer monsoon and the mid-latitude westerlies in Himalayan glaciation: review and speculative discussion, *J. Geol. Soc. London*, 155, 353–363, 1998. 507
- Benn, D. I. and Owen, L. A.: Himalayan glacial sedimentary environments: a framework for reconstructing and dating the former extent of glaciers in high mountains, *Quatern. Int.*, 97–98, 3–25, 2002. 506, 507, 526
- 20 Benn, D., Wiseman, S., and Hands, K.: Growth and drainage of supraglacial lakes on the debris-mantled Ngozumpa Glacier, Khumbu Himal, Nepal, *J. Glaciol.*, 47, 626–638, 2001. 506
- 25 Bishop, M. P. and Shroder Jr J.F., and Hickman, B.: SPOT panchromatic imagery and neural networks for information extraction in a complex mountain environment, *Geocarto Int.*, 14(2), 19–28, 1999. 505
- Bolch, T., Buchroithner, M. F., Kunert, A., and Kamp, U.: Automated delineation of debris-covered glaciers based on ASTER data, in: *Geoinformation in Europe*, in: *Proceedings of 27th EARSeL Symposium*, Bozen, Italy, 4–7 June 2007, 403–410, 2007. 501, 505
- 30 Bolch, T., Buchroithner, M., Pieczonka, T., and Kunert, A.: Planimetric and volumetric glacier changes in the Khumbu Himal, Nepal, since 1962 using Corona, Landsat TM and ASTER data, *J. Glaciol.*, 54, 592–600, 2008a. 507

Optical remote sensing of debris covered glaciersK. A. Casey et al.

[Title Page](#)[Abstract](#)[Introduction](#)[Conclusions](#)[References](#)[Tables](#)[Figures](#)[◀](#)[▶](#)[◀](#)[▶](#)[Back](#)[Close](#)[Full Screen / Esc](#)[Printer-friendly Version](#)[Interactive Discussion](#)

- Bolch, T., Buchroithner, M. F., Peters, J., Baessler, M., and Bajracharya, S.: Identification of glacier motion and potentially dangerous glacial lakes in the Mt. Everest region/Nepal using spaceborne imagery, *Nat. Hazards Earth Syst. Sci.*, 8, 1329–1340, doi:10.5194/nhess-8-1329-2008, 2008. 525
- 5 Bourgeois, C. S., Calanca, P., and Ohmura, A.: A field study of the hemispherical directional reflectance factor and spectral albedo of dry snow, *J. Geophys. Res.*, 111, D20108, doi:10.1029/2006JD007296, 2006. 508
- Bowers, S. A. and Hanks, R. J.: Reflection of radiant energy from soils, *Soil Sci.*, 100, 130–138, 1965. 515
- 10 Buchroithner, M. F. and Bolch, T.: An automated method to delineate the ice extension of the debris-covered glaciers at Mt. Everest based on ASTER imagery, in: 9th International Symposium on High Mountain Remote Sensing Cartography, Graz, Austria, 14–22 September 2006, 71–78, 2006. 501
- Byers, A. C.: An assessment of contemporary glacier fluctuations in Nepal's Khumbu Himal using repeat photography, *Himal. J. Sci.*, 4(6), 21–26, 2007. 507
- 15 Carosi, R., Lombardo, B., Musumeci, G., and Pertusati, P. C.: Geology of the higher Himalayan crystallines in Khumbu Himal (Eastern Nepal), *J. Asian Earth Sci.*, 17, 785–803, 1999. 507
- Casey, K. A., Xie, R., Rysset, O., and Keys, H.: Alpine glaciers in the Himalayas, New Zealand and Norway: investigation of trace elemental abundances, in: International Symposium on Earth's Disappearing Ice, International Glaciological Society, Columbus, Ohio, USA, 15–20 August 2010, 59A029, 2010. 510
- 20 Chen, X., Warner, T. A., and Campagna, D. J.: Integrating visible, near-infrared and short-wave infrared hyperspectral and multispectral thermal imagery for geological mapping at Cuprite, Nevada, *Remote Sens. Environ.*, 110, 344–356, 2007. 523
- 25 Choudhury, B. and Chang, A.: Two-stream theory of reflectance of snow, *IEEE T. Geosci. Elect.*, 17, 63–68, 1979. 513
- Christensen, P. R., Bandfield, J. L., Hamilton, V. E., Howard, D. A., Lane, M. D., Piatek, J. L., Ruff, S. W., and Stefanov, W. L.: A thermal emission spectral library of rock-forming minerals, *J. Geophys. Res.*, 105, 9735–9739, 2000. 505, 547
- 30 Clark, R. N.: *Spectroscopy of Rocks and Minerals, and Principles of Spectroscopy*, vol. 3, John Wiley and Sons, New York, 1999. 547
- Clark, R. N. and Lucey, P. G.: Spectral properties of ice-particulate mixtures and implications for remote sensing 1. Intimate mixtures, *J. Geophys. Res.*, 89, 6341–6348, 1984. 504, 518

Optical remote sensing of debris covered glaciersK. A. Casey et al.

[Title Page](#)[Abstract](#)[Introduction](#)[Conclusions](#)[References](#)[Tables](#)[Figures](#)[◀](#)[▶](#)[◀](#)[▶](#)[Back](#)[Close](#)[Full Screen / Esc](#)[Printer-friendly Version](#)[Interactive Discussion](#)

- Clark, R. N., King, T. V. V., Klejwa, M., Swayze, G. A., and Vergo, N.: High spectral resolution reflectance spectroscopy of minerals, *J. Geophys. Res.*, 95, 12653–12680, 1990. 505
- Clark, R. N., Swayze, G., Wise, R., Livo, E., Hoefen, T., Kokaly, R., and Sutley, S.: USGS spectral library splib06a, available at: <http://speclab.cr.usgs.gov/spectral.lib06>, 23 September 2010, 2007. 514
- 5 Dadon, A., Ben-Dor, E., and Karnieli, A.: Use of derivative calculations and minimum noise fraction transform for detecting and correcting the spectral curvature effect (smile) in Hyperion images, *IEEE T. Geosci. Remote*, 48, 2603–2612, 2010. 518
- Debella-Gilo, M. and Kääb, A.: Sub-pixel precision image matching for measuring surface displacements on mass movements using normalized cross-correlation, *Remote Sens. Environ.*, 115, 130–142, 2011. 512
- 10 Dematte, J. A. M., Campos, R. C., Alves, M. C., Fiorio, P. R., and Nanni, M. R.: Visible-NIR reflectance: a new approach on soil evaluation, *Geoderma*, 121, 95–112, 2004. 523
- Dozier, J.: Spectral signature of alpine snow cover from the landsat thematic mapper, *Remote Sens. Environ.*, 28, 9–22, 1989. 513
- 15 Frauenfelder, R. and Kääb, A.: Towards a palaeoclimatic model of rock-glacier formation in the Swiss Alps, *Ann. Glaciol.*, 31, 281–286, 2000. 501
- Fujii, Y.: Field experiment on glacier ablation under a layer of debris cover, *J. Jap. Soc. Snow Ice*, 39, 20–21, 1977. 501
- 20 Fushimi, H.: Glaciations in the Khumbu Himal, *J. Jap. Soc. Snow Ice*, 40, 71–77, 1978. 525
- Fushimi, H., Yoshida, M., Watanabe, O., and Upadhyay, B.: Distributions and grain sizes of supraglacial debris in the Khumbu glacier, Khumbu Region, East Nepal, *J. Jap. Soc. Snow Ice*, 42, 18–25, 1980. 507, 519, 557
- Gajda, R. T.: Cryoconite phenomena on the Greenland ice cap in the Thule area, *Can. Geogr.*, 12, 35–44, 1958. 514
- 25 Gao, B.-C., Montes, M. J., Davis, C. O., and Goetz, A. F.: Atmospheric correction algorithms for hyperspectral remote sensing data of land and ocean, *Remote Sens. Environ., imaging Spectroscopy Special Issue*, 113, S17–S24, 2009. 518
- Gillespie, A., Kahle, A., and Palluconi, F.: Mapping alluvial fans in Death Valley, California, using multichannel thermal infrared images, *Geophys. Res. Lett.*, 11, 1153–1156, 1984. 505
- 30 Gleeson, D. F., Pappalardo, R. T., Grasby, S. E., Anderson, M. S., Beauchamp, B., Castao, R., Chien, S. A., Doggett, T., Mandrake, L., and Wagstaff, K. L.: Characterization of a sulfur-rich Arctic spring site and field analog to Europa using hyperspectral data, *Remote Sens.*

Optical remote sensing of debris covered glaciers

K. A. Casey et al.

Title Page

Abstract

Introduction

Conclusions

References

Tables

Figures



Back

Close

Full Screen / Esc

Printer-friendly Version

Interactive Discussion



- Environ., 114, 1297–1311, 2010. 518
- Goetz, A. F. H. and Rowan, L. C.: Geologic remote sensing, *Science*, 211, 781–791, 1981. 505
- Goetz, A. F. H., Rock, B. N., and Rowan, L. C.: Remote sensing for exploration, an overview, *Econ. Geol.*, 78, 573–590, 1983. 503, 505
- 5 Govindaraju, K.: 1994 compilation of working values and sample description for 383 geostandards, *Geostandard. Newslett.*, 18, 1–158, 1994. 548
- Griffin, M., Hsu, S., Burke, H., Orloff, S., and Upham, C.: Examples of EO-1Hyperion data analysis, *Lincoln Lab. J.*, 15, 271–298, 2005. 518
- Gupta, R. P.: *Remote Sensing Geology*, 2nd edn., Springer, Berlin, 2003. 505, 515, 521, 547
- 10 Hall, D., Ormsby, J., Bindschadler, R., and Siddalingaiah, H.: Characterization of snow and ice reflectance zones on glaciers using Landsat thematic mapper data, *Ann. Glaciol.*, 9, 104–108, 1987. 524
- Hall, D., Bindschadler, R., Foster, J., Chang, A., and Siddalingaiah, H.: Comparison of in situ and satellite-derived reflectances of Forbindels Glacier, Greenland, *Int. J. Remote Sens.*, 11, 493–504, 1990. 512, 513
- 15 Hall, D., Foster, J., and Chang, A.: Reflectance of snow measured in situ and from space in sub-Arctic areas in Canada and Alaska, *IEEE T. Geosci. Remote*, 30, 634–637, 1992. 508
- Hall, D. K., Chang, A. T., and Siddalingaiah, H.: Reflectances of glaciers as calculated using Landsat-5 Thematic Mapper data, *Remote Sens. Environ.*, 25, 311–321, 1988. 500, 503
- 20 Hall, D. K., Box, J. E., Casey, K. A., Hook, S. J., Shuman, C. A., and Steffen, K.: Comparison of satellite-derived and in-situ observations of ice and snow surface temperatures over Greenland, *Remote Sens. Environ.*, 112, 3739–3749, 2008. 524
- Hambrey, M. J., Quincey, D. J., Glasser, N. F., Reynolds, J. M., Richardson, S. J., and Clemmens, S.: Sedimentological, geomorphological and dynamic context of debris-mantled glaciers, Mount Everest (Sagarmatha) region, Nepal, *Quaternary Sci. Rev.*, 27, 2361–2389, 2008. 506, 507, 508, 525
- 25 Haug, T., Kääb, A., and Skvarca, P.: Monitoring ice shelf velocities from repeat MODIS and Landsat data – a method study on the Larsen C ice shelf, Antarctica Peninsula, and 10 other ice shelves around Antarctica, *The Cryosphere*, 4, 161–178, 2010, <http://www.the-cryosphere-discuss.net/4/161/2010/>. 512
- 30 Hook, S. J., Gabell, A., Green, A., and Kealy, P.: A comparison of techniques for extracting emissivity information from thermal infrared data for geologic studies, *Remote Sens. Environ.*, 42, 123–135, 1992. 505, 522

Optical remote sensing of debris covered glaciers

K. A. Casey et al.

Title Page

Abstract

Introduction

Conclusions

References

Tables

Figures

◀

▶

◀

▶

Back

Close

Full Screen / Esc

Printer-friendly Version

Interactive Discussion



- Hook, S. J., Dmochowski, J. E., Howard, K. A., Rowan, L. C., Karlstrom, K. E., and Stock, J. M.: Mapping variations in weight percent silica measured from multispectral thermal infrared imagery – examples from the Hiller Mountains, Nevada, USA and Tres Virgenes-La Reforma, Baja California Sur, Mexico, *Remote Sens. Environ.*, 95, 273–289, 2005. 523
- 5 Hunt, G. R.: Spectral signatures of particulate minerals in the visible and near infrared, *Geophysics*, 42, 501–513, 1977. 505, 547
- Hunt, G. R. and Salisbury, J. W.: Visible and near-infrared spectra of minerals and rocks – I, silicates, *Mod. Geol.*, 1, 283–300, 1970a. 504
- Hunt, G. R. and Salisbury, J. W.: Visible and near-infrared spectra of minerals and rocks – II, carbonates, *Mod. Geol.*, 2, 23–30, 1970b. 504
- 10 Hunt, G. R., Salisbury, J. W., and Lenhoff, C. J.: Visible and near-infrared spectra of minerals and rocks – III, oxides and hydroxides, *Mod. Geol.*, 2, 195–205, 1971a. 504
- Hunt, G. R., Salisbury, J. W., and Lenhoff, C. J.: Visible and near-infrared spectra of minerals and rocks – IV, sulphides and sulphates, *Mod. Geol.*, 3, 1–14, 1971b. 504
- 15 Kääb, A.: Remote sensing of mountain glaciers and permafrost creep, *Schrift. Phys. Geogr.*, 48, 266 pp., 2005. 501, 506, 518, 520, 549
- Kääb, A. and Vollmer, M.: Surface geometry, thickness changes and flow fields on creeping mountain permafrost: automatic extraction by digital image analysis, *Permafrost Periglac. Process.*, 11, 315–326, 2000. 512
- 20 Kääb, A., Gudmundsson, G. H., and Hoelzle, M.: Surface deformation of creeping mountain permafrost. Photogrammetric investigations of rock glacier Murtel, Swiss Alps, in: *Proceedings of the 7th International Permafrost Conference, Yellowknife, Northwest Territories, Canada, 23–27 June 1998*, 531–537, 1998. 501
- Kadota, T.: Study on the relation between climate and recent shrinkage of small glaciers in the Nepal Himalayas, Ph.D. thesis, Nagoya University, Nagoya, Japan, 1997. 507
- 25 Kadota, T., Seko, K., Oki, T., Iwata, S., and Yamaguchi, S.: Shrinkage of the Khumbu Glacier, East Nepal from 1978 to 1995, *chapt. Debris-covered Glaciers, IAHS, Oxfordshire, UK*, 235–243, 264, 2000. 507
- Kaufman, Y.: The atmospheric effect on remote sensing and its correction, *chapt. Theory and Application of Optical Remote Sensing*, Wiley, New York, 341 pp., 1989. 512
- 30 Kruse, F., Lefkoff, A., Boardman, J., Heidebrecht, K., Shapiro, A., Barloon, P., and Goetz, A.: The spectral image processing system (SIPS) – interactive visualization and analysis of imaging spectrometer data, *Remote Sens. Environ.*, 44, 145–163, 1993. 519, 523

Optical remote sensing of debris covered glaciers

K. A. Casey et al.

Title Page

Abstract

Introduction

Conclusions

References

Tables

Figures



Back

Close

Full Screen / Esc

Printer-friendly Version

Interactive Discussion



- Kruse, F., Boardman, J., and Huntington, J.: Comparison of airborne hyperspectral data and EO-1 Hyperion for mineral mapping, *IEEE T. Geosci. Remote*, 41, 1388–1400, 2003. 517
- Kruse, F. A.: Use of airborne imaging spectrometer data to map minerals associated with hydrothermally altered rocks in the northern grapevine mountains, Nevada, and California, *Remote Sens. Environ.*, 24, 31–51, 1988. 505
- Larsen, C. F., Motyka, R. J., Freymueller, J. T., Echelmeyer, K. A., and Ivins, E. R.: Rapid viscoelastic uplift in Southeast Alaska caused by post-little ice age glacial retreat, *Earth Planet. Sc. Lett.*, 237, 548–560, 2005. 502
- Leprince, S., Barbot, S., Ayoub, F., and Avouac, J.-P.: Automatic and precise orthorectification, coregistration, and subpixel correlation of satellite images, application to ground deformation measurements, *IEEE T. Geosci. Remote*, 45, 1529–1558, 2007. 525
- Liang, S.: *Quantitative Remote Sensing of Land Surfaces*, John Wiley & Sons, Inc., Hoboken, New Jersey, USA, 2004. 515
- Lobell, D. B. and Asner, G. P.: Moisture effects on soil reflectance, *Soil Sci. Soc. Am. J.*, 66, 722–727, 2002. 515
- Lougeay, R.: Detection of buried glacial and ground ice with thermal infrared remote sensing, chap, *Advanced Concepts and Techniques in the Study of Snow and Ice Resources*, An Interdisciplinary Symposium, Monterey, California, USA, 2–6 December 1973, 487–493, 1974. 505
- Lougeay, R.: Landsat thermal imaging of alpine regions, *Photogramm. Eng. Rem. S.*, 48, 269–273, 1982. 505
- Lu, D., Mausel, P., Brondizio, E., and Moran, E.: Assessment of atmospheric correction methods for Landsat TM data applicable to Amazon basin LBA research, *Int. J. Remote Sens.*, 23, 2651–2671, 2002. 512
- Luckman, A., Quincey, D., and Bevan, S.: The potential of satellite radar interferometry and feature tracking for monitoring flow rates of Himalayan glaciers, *Remote Sens. Environ., remote Sensing of the Cryosphere Special Issue*, 111, 172–181, 2007. 525
- Lyon, R. J. P.: Analysis of rocks by spectral infrared emission (8 to 25 microns), *Econ. Geol.*, 60, 715–736, 1965. 504
- MacArthur, A., MacLellan, C., and Malthus, T.: The implications of non-uniformity in fields-of-view of commonly used field spectroradiometers, in: *Geoscience and Remote Sensing Symposium, 2007, IGARSS 2007, Barcelona, Spain, 23–28 July 2007*, IEEE International, 2890–2893, 2007. 509

Optical remote sensing of debris covered glaciers

K. A. Casey et al.

Title Page

Abstract

Introduction

Conclusions

References

Tables

Figures

◀

▶

◀

▶

Back

Close

Full Screen / Esc

Printer-friendly Version

Interactive Discussion



- Markham, B. and Barker, J.: Landsat MSS and TM post-calibration dynamic ranges, exoatmospheric reflectances and at-satellite temperatures, EOSAT Landsat Tech. Notes, 1, 3–8, 1986. 511
- Mars, J. C. and Rowan, L. C.: Spectral assessment of new ASTER SWIR surface reflectance data products for spectroscopic mapping of rocks and minerals, Remote Sens. Environ., 114, 2011–2025, 2010. 512
- Mather, P. M.: Computer Processing of Remotely Sensed Images, John Wiley & Sons, Ltd., Washington, D.C., USA, 1987. 520
- Mattson, L.: The role of debris cover on glacial meltwater discharge, Canadian Rocky Mountains, in: Proceedings of the 47th Eastern Snow Conference, England, 3rd Edn., 237–242, 2004. 501
- Mattson, L.: The influence of a debris cover on the mid-summer discharge of Dome glacier, Canadian Rocky Mountains, chapt. Debris-Covered Glaciers, IAHS, Bangor, Maine, USA, 7–8 June 1990, 25–33, 264, 2000. 501
- Mattson, L., Gardner, J., and Young, G.: Ablation on debris covered glaciers: an example from the Rakhiot glacier, Punjab, Himalaya, IAHS-AISH P, 218, 289–296, 1993. 501
- McClure, D.: The distribution of transition metal cations in spinels, J. Phys. Chem. Solids, 3, 3–4, 1957. 504, 547
- McClure, D.: Electronic spectra of molecules and ions in crystals, Part II. spectra of ions in crystals, Solid State Phys., 9(C), 399–525, 1959. 504, 547
- Meier, M., Dyurgerov, M., Rick, U., O’Neel, S., Pfeffer, W., Anderson, R., Anderson, S., and Glazovsky, A.: Glaciers dominate eustatic sea-level rise in the 21st century, Science, 317, 1064–1067, 2007. 502
- Miyatake, S.: Technical development report: examination of indices for discriminating rocks and minerals and their universal validity, Met. Min. Agency Jap., 3, 1–31, 2000. 522, 559
- Moore, D. M., Reynolds Jr., R. C.: X-ray diffraction and the identification and analysis of clay minerals, 2nd edn., Oxford University Press, New York, 1997. 510
- Nakawo, M., Yabuki, H., and Sakai, A.: Characteristics of Khumbu Glacier, Nepal Himalaya: recent changes in the debris-covered area, Ann. Glaciol., 28, 118–122, 1999. 501, 507, 524
- Nesje, A. and Dahl, S.: Glaciers and Environmental Change, Oxford University Press, Oxfordshire, UK, 2000. 506
- Nicholson, L. and Benn, D.: Calculating ice melt beneath a debris layer using meteorological data, J. Glaciol., 52, 463–470, 2006. 501

Optical remote sensing of debris covered glaciersK. A. Casey et al.

[Title Page](#)[Abstract](#)[Introduction](#)[Conclusions](#)[References](#)[Tables](#)[Figures](#)[Back](#)[Close](#)[Full Screen / Esc](#)[Printer-friendly Version](#)[Interactive Discussion](#)

- Nicodemus, F., Richmond, J., Hsia, J., Ginsberg, I., and Limperis, T.: Geometrical considerations and nomenclature for reflectance, Tech. rep., London, 1977. 509
- Ninomiya, Y.: Rock type mapping with indices defined for multispectral thermal infrared ASTER data: case studies, in: Society of Photo-Optical Instrumentation Engineers (SPIE) Conference Series, vol. 4886, National Bureau of Standards, Monograph 160, Washington, D.C., 123–132, 2003. 520
- Ninomiya, Y.: Lithologic mapping with multispectral ASTER TIR and SWIR data, in: Society of Photo-Optical Instrumentation Engineers (SPIE) Conference Series, vol. 5234, SPIE, Bellingham, Washington, USA, 180–190, 2004. 505, 520
- Ninomiya, Y., Fu, B., and Cudahy, T. J.: Detecting lithology with advanced spaceborne thermal emission and reflection radiometer (ASTER) multispectral thermal infrared radiance-at-sensor data, *Remote Sens. Environ.*, 99, 127–139, 2005. 505, 518, 520, 521, 522, 558
- Nolin, A. W. and Dozier, J.: A hyperspectral method for remotely sensing the grain size of snow, *Remote Sens. Environ.*, 74, 207–216, 2000. 513
- O'Brien, H. and Munis, R.: Red and near-infrared spectral reflectance of snow, in: Operational Applications of Satellite Snowcover Observations, NASA SP-391, proceedings of a workshop held in South Lake Tahoe, California, 345–360, 18–20 August, 1975. 513
- Oerlemans, J., Giesen, R., and van den Broeke, M.: Retreating alpine glaciers: increased melt rates due to accumulation of dust (Vadret da Morteratsch, Switzerland), *J. Glaciol.*, 55, 729–736, 2009. 501
- Ostrem, G.: Ice melting under a thin layer of moraine, and the existence of ice cores in moraine ridges, *Geogr. Ann.*, 41, 228–230, 1959. 501
- Owen, L., Robinson, R., Benn, D., Finkel, R., Davis, N., Yi, C., Putkonen, J., Li, D., and Murray, A.: Quaternary glaciation of Mount Everest, *Quaternary Sci. Rev.*, 28, 1412–1433, 2009. 526
- Painter, T., Duval, B., Thomas, W., Mendez, M., Heintzelman, S. and Dozier, J.: Detection and quantification of snow algae with an airborne imaging spectrometer, *Appl. Environ. Microbiol.*, 67, 5267–5272, 2001. 514, 547
- Painter, T., Paden, B., and Dozier, J.: Automated spectro-goniometer: a spherical robot for the field measurement of the directional reflectance of snow, *Rev. Sci. Instrum.*, 74, 5179–5188, 2003. 508
- Paul, F., Kääb, A., Maisch, M., Kellenberger, T., and Haeberli, W.: The new remote-sensing-derived Swiss glacier inventory. I. methods, *Ann. Glaciol.*, 34, 355–361, 2002. 503

Optical remote sensing of debris covered glaciers

K. A. Casey et al.

Title Page

Abstract

Introduction

Conclusions

References

Tables

Figures

◀

▶

◀

▶

Back

Close

Full Screen / Esc

Printer-friendly Version

Interactive Discussion



- Scherler, D., Leprince, S., and Strecker, M. R.: Glacier-surface velocities in alpine terrain from optical satellite imagery – accuracy improvement and quality assessment, *Remote Sens. Environ.*, 112, 3806–3819, 2008. 525
- Searle, M.: Extensional and compressional faults in the Everest Lhotse massif, Khumbu Himalaya, Nepal, *J. Geol. Soc. London*, 156, 227–240, 1999. 507
- Searle, M., Simpson, R., Law, R., Parrish, R., and Waters, D.: The structural geometry, metamorphic and magmatic evolution of the Everest massif, High Himalaya of Nepal-South Tibet, *J. Geol. Soc. London*, 160, 345–366, 2003. 507, 516
- Seko, K., Yabuki, H., Nakawo, M., Sakai, A., Kadota, T., and Yamada, Y.: Changing surface features of Khumbu Glacier, Nepal Himalayas revealed by SPOT images, *Bull. Glac. Res.*, 16, 33–41, 1998. 525
- Shroder, J. F., Bishop, M. P., Copland, L., and Sloan, V. F.: Debris-covered glaciers and rock glaciers in the Nanga Parbat Himalaya, Pakistan, *Geogr. Ann. A*, 82, 17–31, 2000. 505
- Shukla, A., Arora, M., and Gupta, R.: Synergistic approach for mapping debris-covered glaciers using optical-thermal remote sensing data with inputs from geomorphometric parameters, *Remote Sens. Environ.*, 114, 1378–1387, 2010. 501, 505
- Siegal, B. and Abrams, M.: Geologic mapping using Landsat data, *Photogramm. Eng. Rem. S.*, 42, 325–331, 1976. 515
- Skidmore, E. L., Dickerson, J. D., and Schimmelpfennig, H.: Evaluating surface-soil water content by measuring reflectance, *Soil Sci. Soc. Am. J.*, 39, 238–242, 1975. 515
- Stamnes, K., Li, W., Spurr, R., Eide, H., and Stamnes, J.: Simultaneous retrieval of aerosol and surface properties over bright targets including snow and ice using multi- and hyperspectral data, *Proc. SPIE*, 5569, 56–67, 2004. 512
- Storey, J., Scaramuzza, P., Schmidt, G., and Barsi, J.: Landsat 7 scan line corrector-off gap filled product development, in: *Proceedings of Pecora 16 Global Priorities in Land Remote Sensing*, Sioux Falls, South Dakota, USA, American Society for Photogrammetry and Remote Sensing, 23–27 October 2005, 2005. 503, 511
- Strozzi, T., Paul, F., and Kääb, A.: Glacier mapping with ALOS PALSAR data within the ESA GlobGlacier project, in: *Proceedings of the ESA Living Planet Symposium*, Bergen, Norway 28 June–2 July 2010, 3223, 2010. 501
- Sultan, M., Arvidson, R. E., Sturchio, N. C., and Guinness, E. A.: Lithologic mapping in arid regions with Landsat thematic mapper data: Meatiq dome, Egypt, *Geol. Soc. Am. Bull.*, 99, 748–762, 1987. 505

Optical remote sensing of debris covered glaciers

K. A. Casey et al.

Title Page

Abstract

Introduction

Conclusions

References

Tables

Figures

◀

▶

◀

▶

Back

Close

Full Screen / Esc

Printer-friendly Version

Interactive Discussion



- Suzuki, R., Fujita, K., and Ageta, Y.: Spatial distribution of thermal properties on debris-covered glaciers in the Himalayas derived from ASTER data, *Bull. Glaciol. Res.*, 24, 13–22, 2007. 506
- Takeuchi, N.: Temporal and spatial variations in spectral reflectance and characteristics of surface dust on Gulkana Glacier, Alaska Range, *J. Glaciol.*, 55, 701–709, 2009. 513, 514
- 5 Takeuchi, N. and Li, Z.: Characteristics of surface dust on Urumqi glacier no. 1 in the Tien Shan mountains, China, *Arct. Antarct. Alp. Res.*, 40, 744–750, 2008. 508
- Takeuchi, N., Kohshima, S., and Seko, K.: Structure, formation, and darkening process of albedo-reducing material (cryoconite) on a Himalayan glacier: a granular algal mat growing on the glacier, *Arct. Antarct. Alp. Res.*, 33, 115–122, 2001. 514
- 10 Takeuchi, Y., Kayastha, R., and Nakawo, M.: Characteristics of ablation and heat balance in debris-free and debris-covered areas on Khumbu glacier, Nepal Himalayas, in the pre-monsoon season, in: *Debris-Covered Glaciers*, IAHS, Oxfordshire, UK, 53–61, 2000. 501
- Tamisiea, M. E., Mitrovica, J. X., Milne, G. A., and Davis, J. L.: Global geoid and sea level changes due to present-day ice mass fluctuations, *J. Geophys. Res.*, 106, 30849–30863, 2001. 502
- 15 Tanre, D., Deroo, C., Duhaut, P., Herman, M., Morcrette, J., Perbos, J., and Deschamps, P.: Description of a computer code to simulate the satellite signal in the solar spectrum: the 5S code, *Int. J. Remote Sens.*, 11, 659–668, 1990. 512
- Taschner, S. and Ranzi, R.: Comparing the opportunities of Landsat-TM and Aster data for monitoring a debris covered glacier in the Italian Alps within the GLIMS project, *Int. Geosci. Remote Se.*, 2, 1044–1046, 2002. 501, 505
- 20 Tucker, C. J., Grant, D. M., and Dykstra, J. D.: NASA's global orthorectified Landsat data set, *Photogramm. Eng. Rem. S.*, 70, 313–322, 2004. 511
- Vincent, R. and Thomson, F.: Rock-type discrimination from ratioed infrared scanner images of Pissgah Crater, California, *Science*, 175, 986–988, 1972. 505, 520
- 25 Wang, T., Yan, G., Ren, H., and Mu, X.: Improved methods for spectral calibration of on-orbit imaging spectrometers, *IEEE T. Geosci. Remote*, 48, 3924–3931, 2010. 518
- Warren, S.: Optical Properties of Snow, *Rev. Geophys. Space Ge.*, 20, 67–89, 1982. 513, 514
- Warren, S. and Wiscombe, W.: A model for the spectral albedo of snow. II: snow containing atmospheric aerosols, *J. Atmos. Sci.*, 37, 2734–2745, 1980. 501, 514
- 30 Watanabe, H. and Matsuo, K.: Rock type classification by multi-band TIR of ASTER, *Geosci. J.*, 7, 347–358, 2003. 522
- Wessels, R., Kargel, J., and Kieffer, H.: ASTER measurement of supraglacial lakes in the Mount

- Everest region of the Himalaya, *Ann. Glaciol.*, 34, 399–408, 2002. 506, 507
- Wiens, R. C., Arvidson, R. E., Cremers, D. A., Ferris, M. J., Blacic, J. D., Seelos, Frank, P. I., and Deal, K. S.: Combined remote mineralogical and elemental identification from rovers: field and laboratory tests using reflectance and laser-induced breakdown spectroscopy, *J. Geophys. Res.*, 107, 8004, 2002. 508
- 5 Winther, J.-G.: Landsat TM derived and in situ summer reflectance of glaciers in Svalbard, *Polar Res.*, 12, 37–55, 1993. 513
- Wiscombe, W. J. and Warren, S. G.: A model for the spectral albedo of snow. I: pure snow, *J. Atmos. Sci.*, 37, 2712–2733, 1980. 513
- 10 Yao, T.: Glacial retreat and its impact on hydrological processes on the third pole, in: International Symposium on Earth's Disappearing Ice, International Glaciological Society, Columbus, Ohio, USA, 15–20 August 2010, 59A100, 2010. 502
- Yoshimura, Y., Kohshima, S., Takeuchi, N., Seko, K., and Fujita, K.: Himalayan ice-core dating with snow algae, *J. Glaciol.*, 46, 335–340, 2000. 514
- 15 Zheng, L., Li, M., Sun, J., Zhang, X., and Zhao, P.: Estimating soil moisture based on image processing technologies, *Proc. SPIE*, San Diego, CA, USA, 5909, 548–555, 2005. 515

Optical remote sensing of debris covered glaciers

K. A. Casey et al.

Title Page

Abstract

Introduction

Conclusions

References

Tables

Figures

◀

▶

◀

▶

Back

Close

Full Screen / Esc

Printer-friendly Version

Interactive Discussion



Optical remote sensing of debris covered glaciers

K. A. Casey et al.

Table 2. A listing of the satellite products and scene dates used for the optical remote sensing methods evaluated in this study.

Comparison method	Sensor, data product	Date(s) of scene(s), further details
Satellite derived reflectance		
multispectral	ASTER, AST_07XT	29 Nov 2005
hyperspectral	Hyperion, L1T	13 May 2002, 4 Oct 2010
True and false color composites		
	ALI, L1T	4 Oct 2010, 10 m pan enhanced true color
	ASTER, L1B	29 Nov 2005, SWIR/TIR false color
	Landsat TM, L1T	31 Oct 2009, true color
	Landsat ETM+, L1G	24 Jan 2003, SWIR/TIR false color
	Hyperion, L1T	13 May 2002, true color, SWIR false color
Mineralogic mapping:		
SWIR/TIR indices	ASTER, L1B	29 Nov 2005
SiO ₂ weight percent	ASTER, AST_05	29 Nov 2005
Spectral Angle Mapper	ASTER, L1B, AST_07XT	29 Nov 2005
Land surface temperature		
	Landsat TM, L1T	31 Oct 2009
	ASTER, AST_08	29 Nov 2005
Glacier velocity, streamlines		
	Landsat TM, L1T	5 Nov 2005, 31 Oct 2009, 30 m near infrared
	Landsat ETM+, L1G	30 Oct 2000, 4 Oct 2002, 15 m pan

Title Page

Abstract

Introduction

Conclusions

References

Tables

Figures

◀

▶

◀

▶

Back

Close

Full Screen / Esc

Printer-friendly Version

Interactive Discussion



Optical remote sensing of debris covered glaciers

K. A. Casey et al.

Table 3. In situ and satellite comparison of mineralogy and silica abundance at Ngozumpa and Khumbu glacier sample locations. XRD-derived minerals are listed in order of greatest abundance per sample. XRF SiO₂ weight percent and ASTER TIR estimated Eq. (7) SiO₂ composition are also listed. ASTER TIR SiO₂ weight percent is averaged from the nearest two 90 m pixels to the in situ sample site. In situ geochemical results compare generally well with the satellite derived estimates.

Sample ID	Debris type	XRD determined mineral classes in order of abundance	XRF derived SiO ₂	ASTER TIR estimated SiO ₂
1N	mud	quartz, feldspar, mica, K-feldspar, calcite	66.3	72.8
2N	mud	quartz, feldspar, mica, K-feldspar, calcite	66.4	
3N	sand	mica, quartz, feldspar, K-feldspar, calcite	62.7	70.7
4N	sand	quartz, mica, feldspar, K-feldspar, calcite	65.1	
5N	gravel	feldspar, quartz, K-feldspar, mica, calcite	71.9	77.9
6N	gravel	mica, feldspar, quartz, microcline, clinochlore	62.5	
7N	rock	feldspar, feldspar, calcite, quartz, K-feldspar	37.2	58.6
8N	rock	calcite, wollastonite	6.6	
9K	mud	mica, feldspar, quartz, microcline, clinochlore	61.4	78.7
10K	mud	mica, feldspar, quartz, K-feldspar, nimite	62.0	
11K	rock	phlogopite, feldspar, anorthite, quartz, nimite	63.8	58.6
12K	rock	feldspar, mica, phlogopite, quartz, clinochlore	54.1	
13K	rock	calcite, feldspar, quartz	7.1	58.6
14K	sand	quartz, feldspar, microcline, mica, mica	71.5	
15K	sand	feldspar, quartz, K-feldspar, mica	71.7	58.6
16K	soil	feldspar, feldspar, quartz, K-feldspar, mica, illite	71.1	
17K	soil	feldspar, quartz, mica, K-feldspar	68.1	58.6
18K	soil	mica, quartz, feldspar, K-feldspar, nimite	69.2	
19K	gravel	mica, quartz, feldspar, clinochlore, K-feldspar	63.1	58.6
20K	gravel	mica, quartz, feldspar, ankerite, nimite	61.0	
21K	sand	phlogopite, quartz, feldspar, microcline, clinochlore	63.5	58.6
22K	sand	mica, feldspar, quartz, microcline, calcite, nimite	62.8	

[Title Page](#)
[Abstract](#)
[Introduction](#)
[Conclusions](#)
[References](#)
[Tables](#)
[Figures](#)
[Back](#)
[Close](#)
[Full Screen / Esc](#)
[Printer-friendly Version](#)
[Interactive Discussion](#)


Optical remote sensing of debris covered glaciers

K. A. Casey et al.

Table A1. Characteristic absorption feature values after Hunt (1977); Clark (1999); Gupta (2003) unless otherwise noted.

Wavelength	Component	Absorption feature (μm)
VNIR	Mg ³⁺	1.0
	Cr ³⁺	0.4, 0.55, 0.7
	Mn ²⁺	0.34, 0.37, 0.41, 0.45, 0.55 (McClure, 1959)
	Fe ³⁺ , Fe ²⁺	0.44, 0.87, 0.95
	Ni ²⁺	0.4, 0.74, 1.25 (McClure, 1957)
	Cu ²⁺	0.8
	Rare Earth Ions, La ²⁺	0.5, 0.58
	Atmospheric O ₂ , Atmospheric H ₂ O	0.76, 0.94
	Water, Snow, Ice	0.98, 0.90, 1.03
	Algal snow	0.55, 0.68 (Painter et al., 2001)
SWIR	Carbonates	1.9, 2.35, 2.55
	Hydroxides, (Al-OH, Mg-OH)	2.7, overtone at 1.44, (2.2, 2.3)
	Water vapor	1.4, 1.7
	Snow	1.03, 1.25, 1.50
TIR	Chlorites	7.0
	Silicates	8.5–12.0 (e.g.: 8.7, 9.7 microcline; 9.2, 10.2 wollastonite; 10.0 hornblende) (Christensen et al., 2000)
	Carbonates	11.3 (11.4 calcite, 11.2 dolomite)
	Sulfates	9.0, 16.0
	Phosphates	9.25, 13.3
	Hydroxides	11.0

Title Page

Abstract

Introduction

Conclusions

References

Tables

Figures

◀

▶

◀

▶

Back

Close

Full Screen / Esc

Printer-friendly Version

Interactive Discussion



Table B1. In situ collected samples X-ray fluorescence (XRF) determined major oxide percent weights and part per million concentrations of trace elements. The locations and types of samples gathered are listed in Table 1, and mapped in Figs. 3 and 9. (XRF measurement accuracy is 98%. Basalt (BE-N, JB-1a, JB-2), diorite (DR-N) and disthene (DT-N) standards (after Govindaraju, 1994)) were utilized for XRF quality control. Over 100 total standards were used for XRF calibration.

Sample ID	SiO ₂	Al ₂ O ₃	Fe ₂ O ₃	MgO	CaO	Na ₂ O	K ₂ O	V	Co	Zn	Pb	Zr	Th	U
1N	66.26	14.79	4.58	1.69	2.34	2.99	4.12	56	15	90	42	194	21	10
2N	66.38	14.69	4.85	1.70	2.34	2.96	4.10	56	17	92	42	188	19	11
3N	62.73	14.89	4.79	1.86	2.27	2.74	4.23	54	13	96	43	204	21	11
4N	65.09	13.10	3.42	1.28	2.29	2.94	3.77	37	10	69	40	174	18	7
5N	71.88	13.00	1.16	0.10	2.09	4.24	3.79	1	4	30	50	51	5	14
6N	62.45	14.34	6.42	2.55	2.19	2.29	4.60	79	19	84	27	309	26	6
7N	43.41	8.75	0.83	0.37	23.26	2.91	1.03	14	2	15	38	109	9	13
8N	10.21	1.90	1.80	0.83	48.61	0.01	0.23	19	4	34	13	90	5	10
9K	61.41	17.26	5.39	2.12	1.98	2.32	4.85	73	14	103	38	218	20	15
10K	61.96	17.80	5.79	2.25	1.89	2.33	4.98	82	18	107	37	233	22	17
11K	63.78	13.76	6.38	2.73	2.57	2.79	3.02	76	19	96	37	235	22	4
12K	54.08	18.94	7.42	3.00	5.40	3.33	2.83	130	18	108	30	450	38	9
13K	7.34	1.12	0.54	0.49	49.3	0.46	0.11	8	0	16	391	94	–	13
14K	71.52	12.28	2.63	0.57	2.86	3.73	2.85	23	5	179	40	151	10	12
15K	71.69	13.55	1.22	0.14	0.71	4.14	4.53	5	2	39	51	62	7	15
16K	71.08	13.32	1.41	0.22	0.86	3.69	4.62	8	1	27	55	83	10	8
17K	68.14	13.49	2.95	0.91	1.54	3.24	4.13	31	8	50	40	145	14	9
18K	69.21	11.78	5.35	2.18	2.75	1.90	3.30	72	14	71	24	501	28	7
19K	63.14	14.82	6.14	2.64	2.96	2.05	3.78	79	17	98	26	251	21	6
20K	61.01	14.24	6.24	2.73	3.47	1.96	3.48	78	17	95	30	289	22	7
21K	63.50	14.62	5.14	2.24	2.59	2.24	4.24	64	16	84	32	202	17	7
22K	62.82	14.59	5.39	2.36	2.57	2.19	4.18	71	17	82	33	209	18	8

Optical remote sensing of debris covered glaciers

K. A. Casey et al.

Title Page

Abstract

Introduction

Conclusions

References

Tables

Figures

◀

▶

◀

▶

Back

Close

Full Screen / Esc

Printer-friendly Version

Interactive Discussion



Optical remote sensing of debris covered glaciers

K. A. Casey et al.

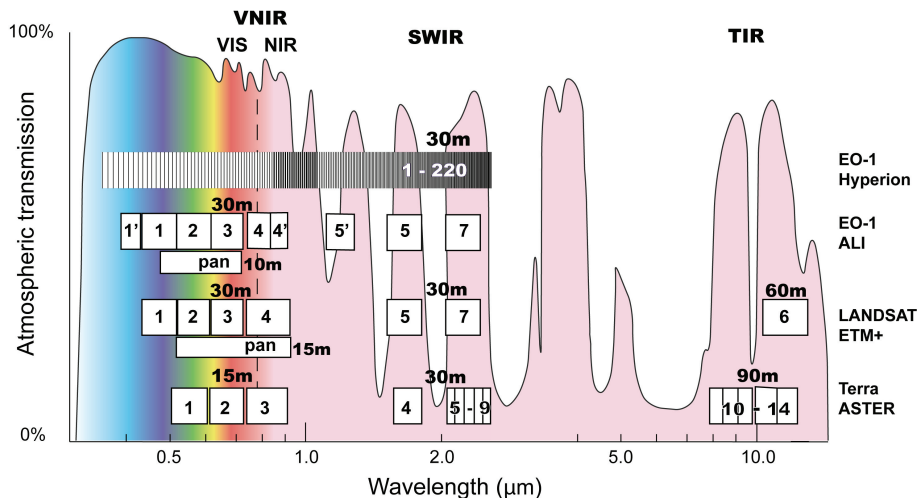


Fig. 1. Spectral coverage of Hyperion, ASTER and Landsat ETM+ sensors with regard to atmospheric transmission in the visible to thermal infrared wavelength range (Adapted after Kääb, 2005).

Discussion Paper | Discussion Paper | Discussion Paper | Discussion Paper | Discussion Paper

Title Page

Abstract Introduction

Conclusions References

Tables Figures

◀ ▶

◀ ▶

Back Close

Full Screen / Esc

Printer-friendly Version

Interactive Discussion



Optical remote sensing of debris covered glaciers

K. A. Casey et al.



Fig. 2. Overview map of study region, with the Khumbu Himalaya, Nepal area highlighted by the yellow box. (Background image courtesy of MODIS based NASA Earth Observatory Blue Marble.)

[Title Page](#)[Abstract](#)[Introduction](#)[Conclusions](#)[References](#)[Tables](#)[Figures](#)[◀](#)[▶](#)[◀](#)[▶](#)[Back](#)[Close](#)[Full Screen / Esc](#)[Printer-friendly Version](#)[Interactive Discussion](#)

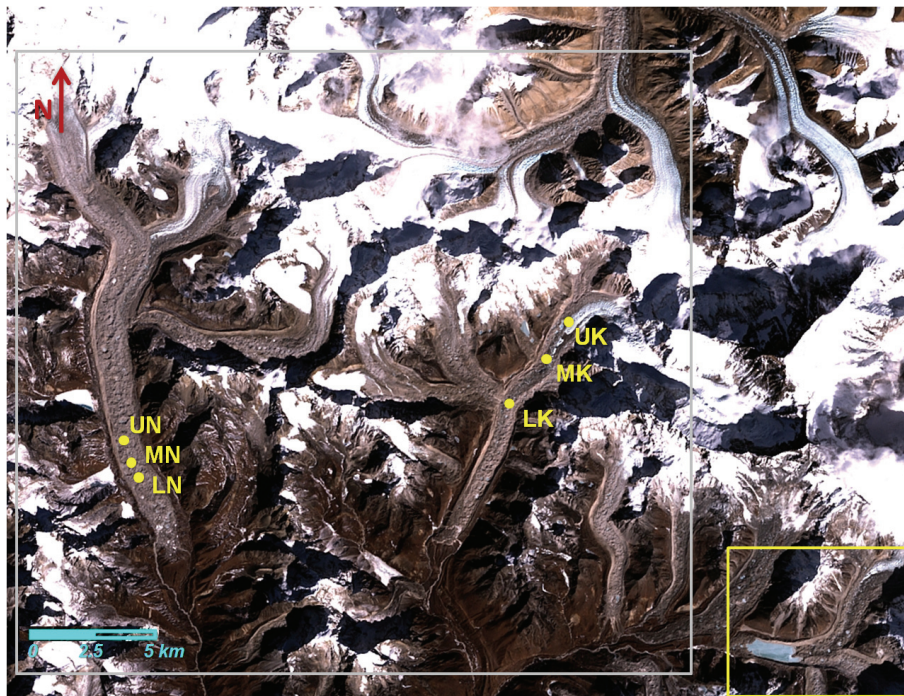


Fig. 3. Landsat TM true color composite (31 October 2009, Bands 3, 2, 1) of the Khumbu Himalaya study area. Ngozumpa glacier (left) and Khumbu glacier (right) in situ measurement locations are labeled as follows: Upper Ngozumpa – UN, Mid-Ngozumpa – MN, Lower Ngozumpa – LN, Upper Khumbu – UK, Mid-Khumbu – MK, Lower Khumbu – LK. The approximate area of comparison mapped in (Figs. 9, 11 and 14) is highlighted by the gray box. The approximate area presented in the Hyperion Imja and Lhotse Shar glacier analysis is highlighted with a yellow box in the lower right hand corner.

Optical remote sensing of debris covered glaciers

K. A. Casey et al.

Discussion Paper | Discussion Paper | Discussion Paper | Discussion Paper | Discussion Paper

Title Page	
Abstract	Introduction
Conclusions	References
Tables	Figures
◀	▶
◀	▶
Back	Close
Full Screen / Esc	
Printer-friendly Version	
Interactive Discussion	



Optical remote sensing of debris covered glaciers

K. A. Casey et al.

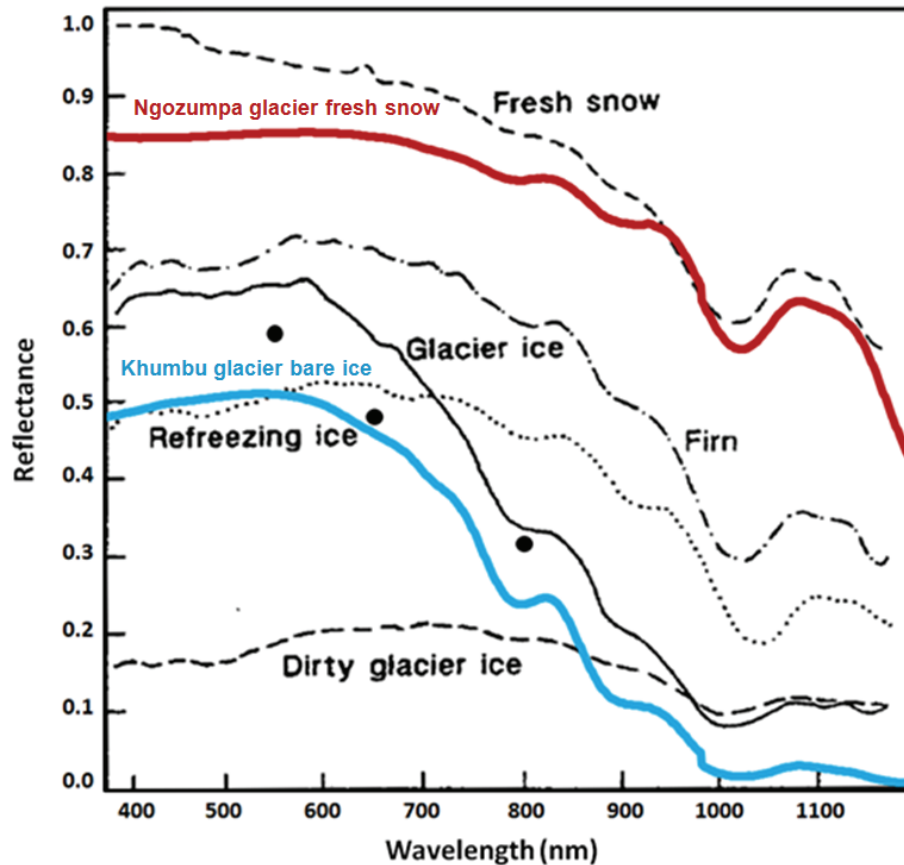


Fig. 4. Field spectra of Ngozumpa glacier fresh snow (red) and Khumbu glacier bare ice (cyan) measurements as compared to reference snow and ice spectral signatures by Qunzhu et al. (1985), ASTER derived surface reflectance values for the Khumbu glacier bare ice are over plotted in black circles. (Qunzhu et al. (1985) graph reprinted with permission from IAHS.)

Title Page

Abstract

Introduction

Conclusions

References

Tables

Figures

◀

▶

◀

▶

Back

Close

Full Screen / Esc

Printer-friendly Version

Interactive Discussion



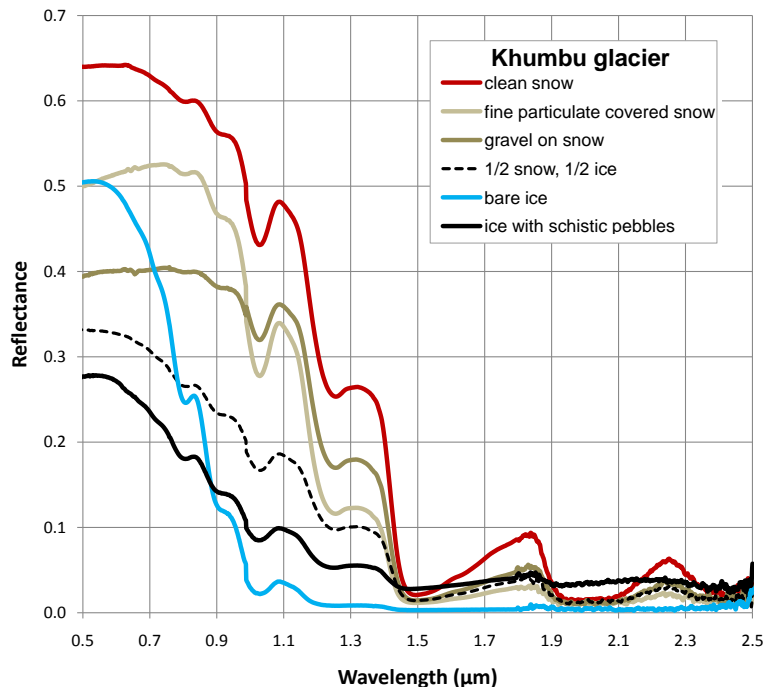


Fig. 5. Khumbu glacier clean snow, fine particulate covered snow, gravel on snow, mixed pixel half snow, half ice and bare ice spectra are plotted that were acquired in the ice pinnacles region near the Khumbu icefall. Spectral signatures represent an average of 20 individual spectral measurements. Particulate and gravel covered snow reduces reflectivity in the visible portion of the spectrum, with debris composition beginning to be expressed in the gravel on snow signature (see reference spectral signature for sillimanite gneiss in Appendix A). The mixed pixel (half snow, half ice) spectral measurements result in a change in the slope of the reflectance from visible to near infrared. Clean snow and bare ice spectral acquisitions are displayed for comparison.

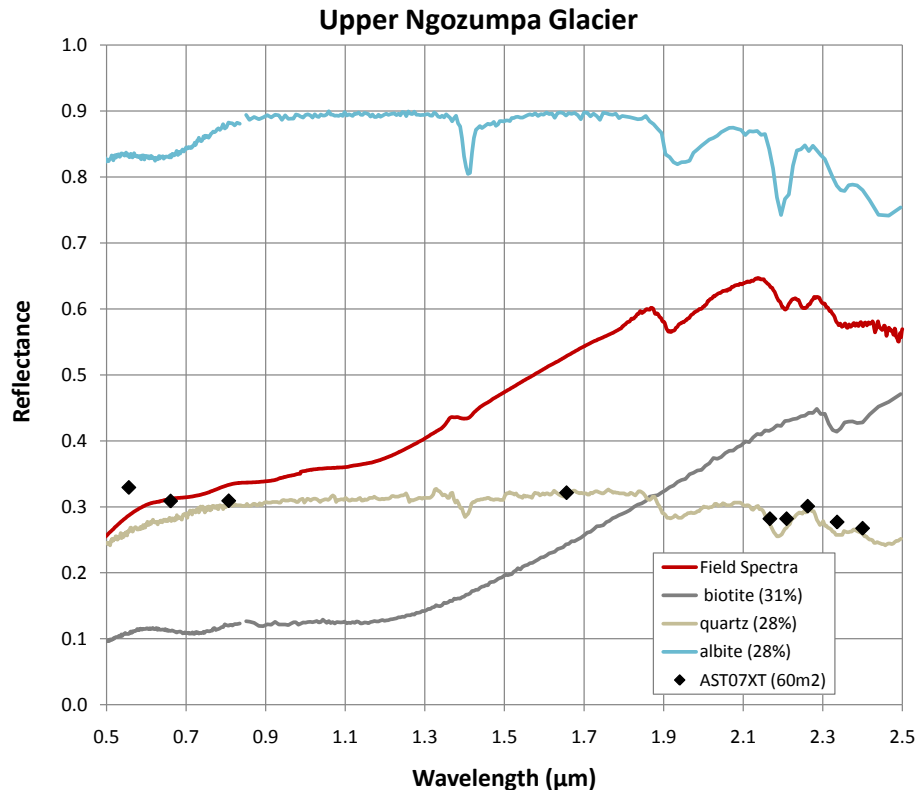


Fig. 6. Upper Ngozumpa glacier collected spectral signature of debris from 27 November 2009, corresponding with sample 3N of sand. Field measured reflectance is plotted in red along with spectral library reference reflectances of the 3 major minerals determined by XRD analysis: biotite (31%), quartz (28%), and albite (28%) (ASTER spectral library reference numbers: USGS231-HS28, AP-958-111, and USGS231-HS324, respectively). Corresponding ASTER (AST_07XT) surface reflectance (60 m² comparison – 4 × 4 pixels in visible bands 1–3, 2 × 2 pixels in SWIR bands 4–9) from 29 November 2005 is over plotted in black diamonds.

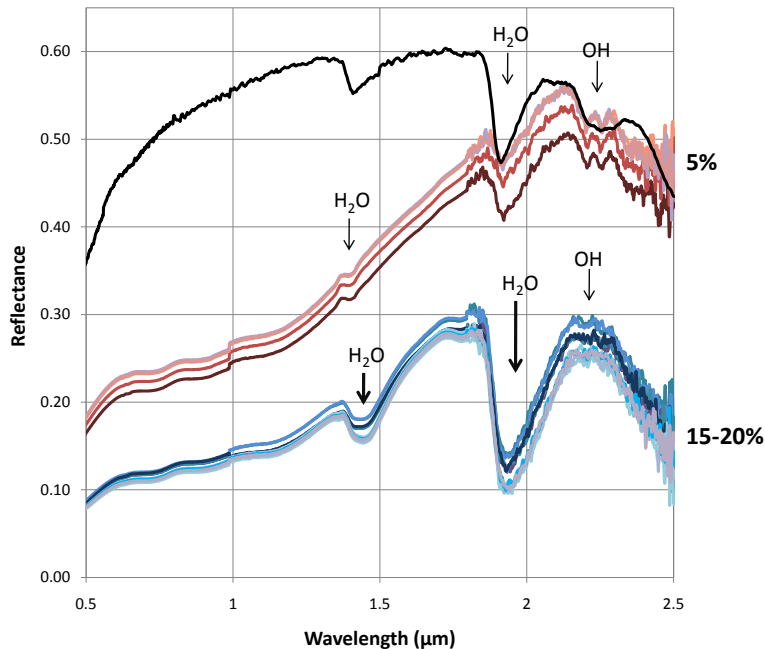


Fig. 7. Graph of two sets of reflectance field spectra acquired on 27 November 2009 at the upper Ngozumpa glacier site over mud of varying degrees of moisture (corresponding with debris sample ID's 1N, 2N). The set of spectra plotted by the red hues was visibly drier than the set of spectra plotted by blue hues. A spectral library reference reflectance profile of the dominant mineral determined by XRD analysis, quartz, is over plotted in black (ASTER spectral library No.382). Water content in the upper set of spectra is estimated at 5%, and 15–20% in the lower set of spectra. Water absorption bands are shown at 1.4 and 1.9 μm, and hydroxyl absorption at 2.2 μm. Water absorption features increase with greater moisture content and conversely, hydroxyl absorption decreases with increasing moisture. While sediment grain size is a factor in the intensity of the reflectance, moisture content dominates the intensity of the signal.

Optical remote sensing of debris covered glaciers

K. A. Casey et al.

Title Page

Abstract Introduction

Conclusions References

Tables Figures

◀ ▶

◀ ▶

Back Close

Full Screen / Esc

Printer-friendly Version

Interactive Discussion



Optical remote sensing of debris covered glaciers

K. A. Casey et al.

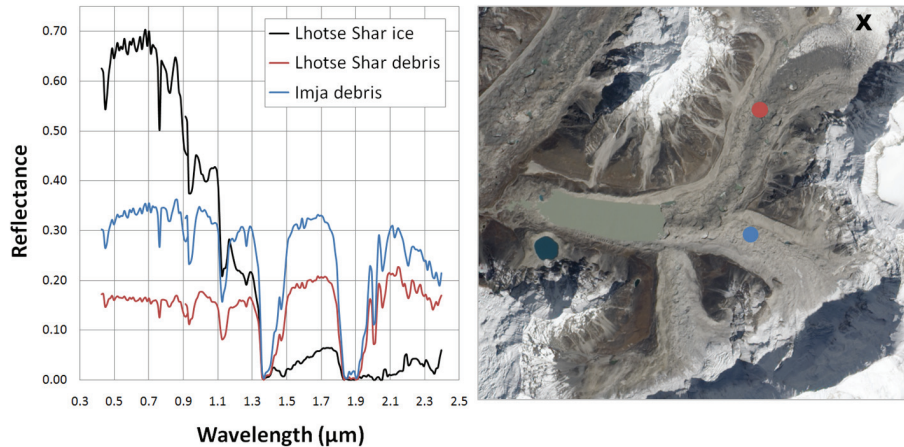


Fig. 8. Hyperion (13 May 2002) derived at-sensor reflectance plot (left) of Imja glacier debris (blue) vs. Lhotse Shar glacier debris (red) spectral signatures with a Lhotse Shar ice spectral signature shown for reference (black). An ALI (4 October 2010) 10 m pan-enhanced true color composite is shown on the right (courtesy NASA Earth Observatory) with the locations of the Hyperion derived spectra for debris shown in blue and red dots and ice in the black X.

Title Page

Abstract

Introduction

Conclusions

References

Tables

Figures

◀

▶

◀

▶

Back

Close

Full Screen / Esc

Printer-friendly Version

Interactive Discussion



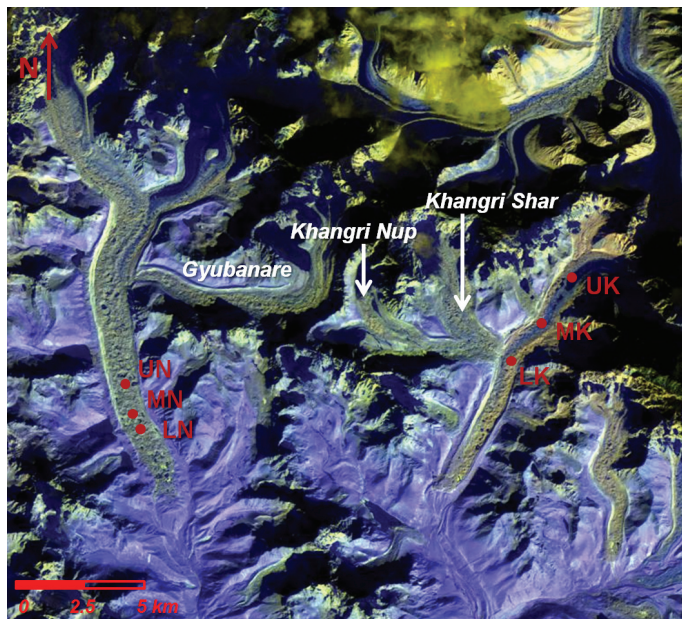


Fig. 9. SWIR, TIR Landsat bands (5, 7, 6) (1.65, 2.2, 11 μm) false color composite from 24 January 2003 displaying geologic differences of Ngozumpa, Khumbu and Imja glacier debris. Silicon dioxide rich granites are indicated by yellow coloring, while the blue color highlights strong amounts of gneiss. The Khumbu glacier longitudinal schistic supraglacial debris band reported by Fushimi et al. (1980) can be visualized in blue in this false color composite, as well as similar longitudinal supraglacial debris bands on upper Ngozumpa glacier. Indication of limited mass flux can be seen by the distinct change in supraglacial composition that can be visualized at the confluence of the Khangri Shar, Khangri Nup and Khumbu glacier – negligible mass is input to the Khumbu glacier. A difference in supraglacial debris on Ngozumpa vs. Khumbu glacier can be visualized, XRD-derived mineralogy found Ngozumpa in situ samples to be quartz, feldspar and mica dominant vs. Khumbu in situ samples that were mica, feldspar and quartz dominant.

Optical remote sensing of debris covered glaciers

K. A. Casey et al.

Title Page

Abstract

Introduction

Conclusions

References

Tables

Figures

◀

▶

◀

▶

Back

Close

Full Screen / Esc

Printer-friendly Version

Interactive Discussion



Optical remote sensing of debris covered glaciers

K. A. Casey et al.

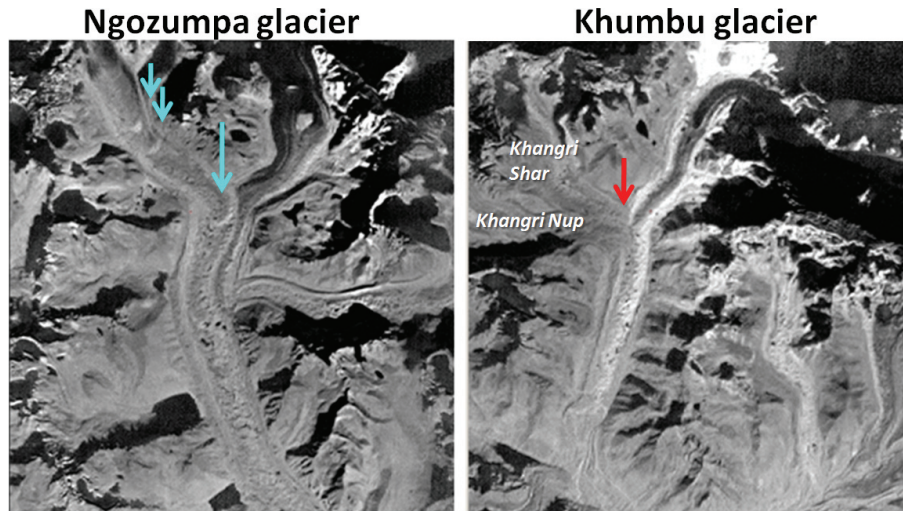


Fig. 10. ASTER (L1B radiance data 29 November 2005) SWIR based silicate index (Eq. 2) after Ninomiya et al. (2005) images of Ngozumpa glacier (left) and Khumbu glacier (right): darker shades indicate lower amounts of silicates, brighter shades indicate higher amounts of silicates. Cyan arrows on the Ngozumpa glacier point to areas of pulse like flow that are made more evident by the silicate index. The red arrow on the Khumbu glacier highlights the distinct transition in debris type at the convergence of the Khangri Shar, Khangri Nup and Khumbu glaciers. The Khumbu glacier longitudinal non-silicate rich schist band vs. the lateral longitudinal glacier silicate-rich granite bands are evident.

Title Page

Abstract

Introduction

Conclusions

References

Tables

Figures

◀

▶

◀

▶

Back

Close

Full Screen / Esc

Printer-friendly Version

Interactive Discussion



Optical remote sensing of debris covered glaciers

K. A. Casey et al.

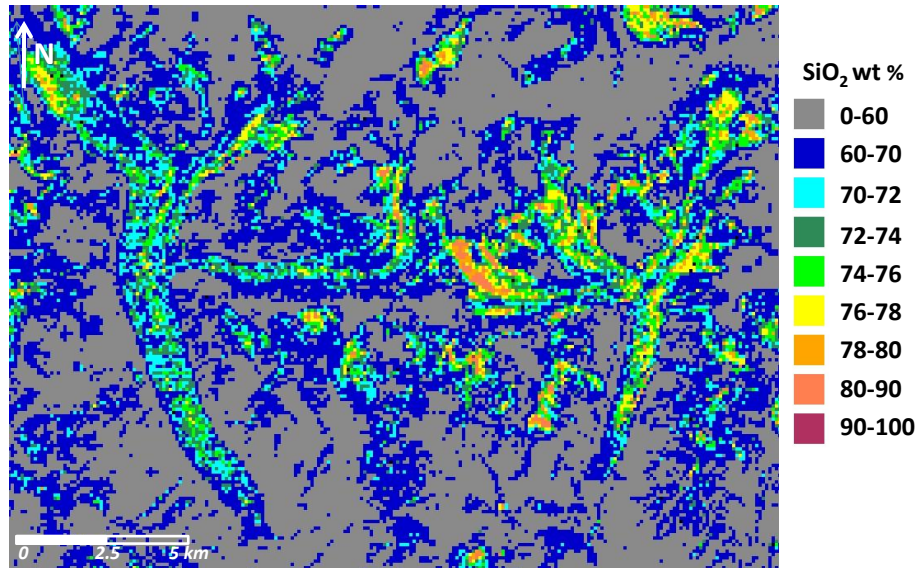


Fig. 11. SiO₂ weight percent distribution thematic map based on ASTER thermal emissivity bands after Miyatake (2000). Debris covered glacier areas are evident by elevated SiO₂ content in this region, perhaps due to the high supraglacial activity in terms of sediment transport, deposition and glacial erosion.

Title Page

Abstract

Introduction

Conclusions

References

Tables

Figures

◀

▶

◀

▶

Back

Close

Full Screen / Esc

Printer-friendly Version

Interactive Discussion



Optical remote sensing of debris covered glaciers

K. A. Casey et al.

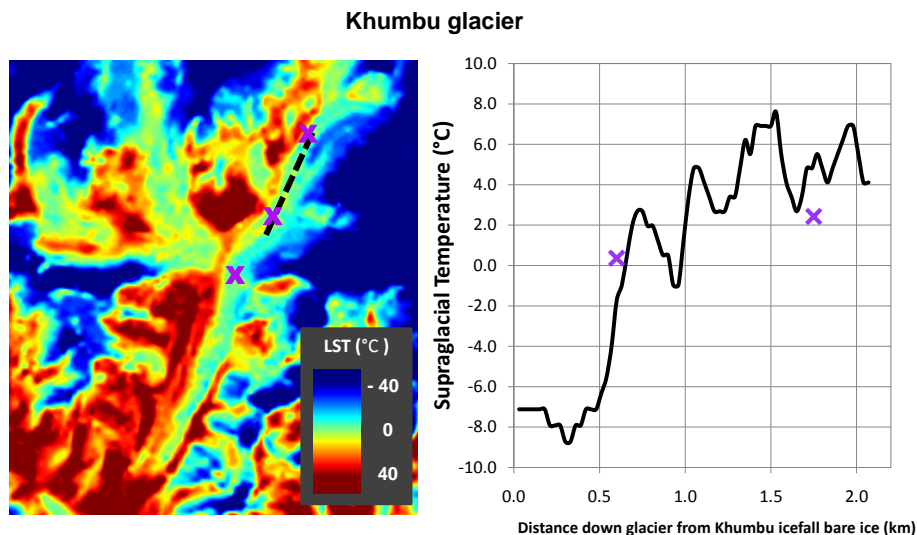


Fig. 12. Khumbu glacier regional Landsat TM (31 October 2009) derived surface temperature map is displayed on the left. A graph showing a surface temperature transect down glacier is shown on the right. In situ ground temperature measurements are indicated on the map and graph by the purple “X” annotations. Glacier surface temperature increases approximately 15°C two kilometers down glacier from the Khumbu icefall. In situ average temperatures of 0.4°C for upper Khumbu, 2.4°C for mid-Khumbu, and 6.7°C for lower Khumbu sample sites relate to Landsat TM LST’s of –3.2, 4.8, 3.4°C, respectively.

[Title Page](#)
[Abstract](#)
[Introduction](#)
[Conclusions](#)
[References](#)
[Tables](#)
[Figures](#)
[◀](#)
[▶](#)
[◀](#)
[▶](#)
[Back](#)
[Close](#)
[Full Screen / Esc](#)
[Printer-friendly Version](#)
[Interactive Discussion](#)


Optical remote sensing of debris covered glaciers

K. A. Casey et al.

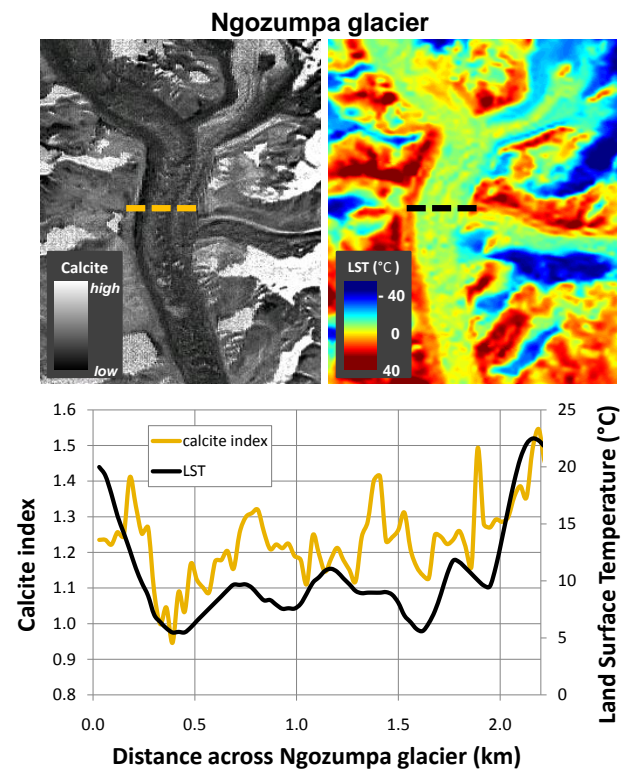


Fig. 13. The top portion of the image shows a ASTER L1B (29 November 2005) derived calcite index Eq. (3, left), and a Landsat TM (31 October 2009) derived LST map of Ngozumpa glacier study area. The graph below shows transect values of calcite index (light brown) and LST (blue) across the upper Ngozumpa ablation area. It may be possible to analyze ablation rate influences of different mineral types, for example as shown in the transect graph in the lower portion of the image, calcite rich areas correspond with higher glacier surface temperatures.

Title Page

Abstract Introduction

Conclusions References

Tables Figures

◀ ▶

◀ ▶

Back Close

Full Screen / Esc

Printer-friendly Version

Interactive Discussion



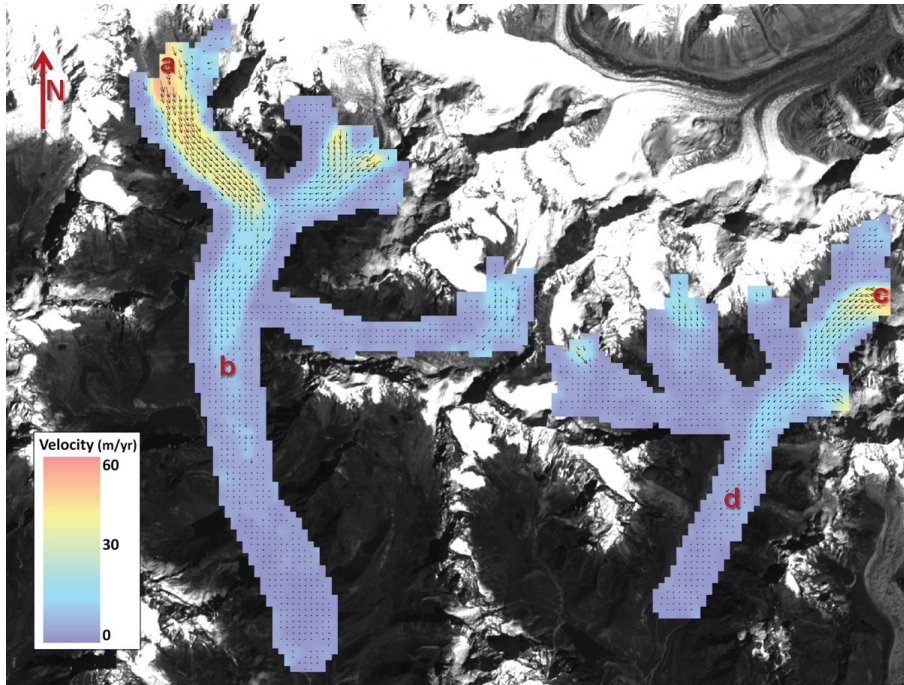


Fig. 14. Glacier surface velocity and flow directions are presented for Ngozumpa (left) and Khumbu (right) glaciers based on repeat feature tracking of Landsat ETM+ 15 m pan band images (30 October 2000, 4 October 2002). Velocity shown in meter per year displacement (by color) and flow direction (by black arrows). Theoretical supraglacial particulate streamline estimate the travel time from a to b on Ngozumpa glacier at 380 years, and travel time from c to d on Khumbu glacier at 450 years. The streamline interpolation stops where velocities are below the error margin of around 4 m/yr. So, the ages from streamlines are minimum ages. (Background image is Landsat ETM+ 15 m pan band from 4 October 2002.)

Optical remote sensing of debris covered glaciers

K. A. Casey et al.

Title Page	
Abstract	Introduction
Conclusions	References
Tables	Figures
◀	▶
◀	▶
Back	Close
Full Screen / Esc	
Printer-friendly Version	
Interactive Discussion	



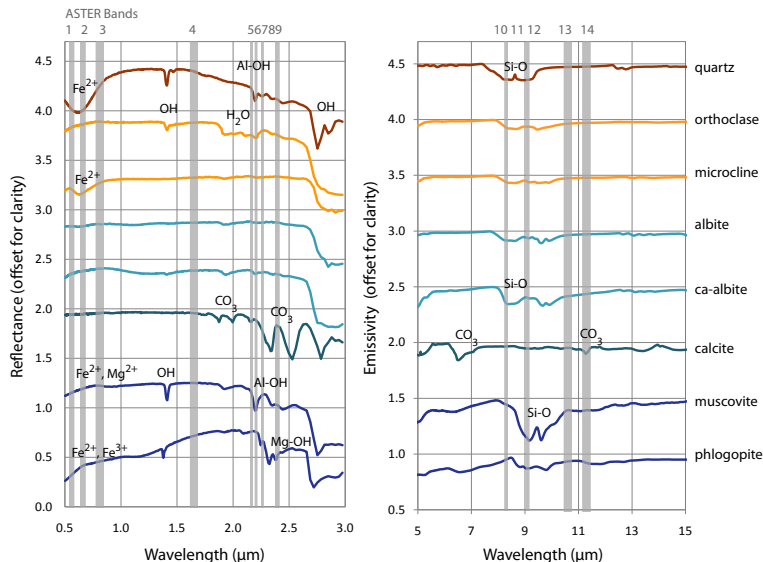


Figure A1. Reflective (VNIR-SWIR, left plot) and emissive (TIR, right plot) reference spectral library mineral signatures are displayed with ASTER multispectral band wavelength positions over plotted in gray. A y-axis offset of 0.5 has been applied to the mineral spectra for visualization purposes (maximum reflectance of spectra is 1). Emissivity values were calculated using Kirchoff's Law ($E = 1 - R$) where E is emissivity and R is reflectance. Note that measurements are from the USGS spectral library of specimens collected in different regions, at different grain sizes, and measured with differing laboratory conditions. Hence, signatures should be visualized with respect to general shape and potential characteristic features – which can be modified with substitution of different cations, among other factors). (Specific ASTER and USGS VNIR-SWIR and TIR spectral library references: quartz HS117.3B-5842, 32B; orthoclase HS13.3B, NMNH113188; microcline NMNH135231; albite GDS30-144, NMNHC5390; Ca-albite HS143.3B-5025, HS143.3B-3176; calcite WS272-1520, 194B; muscovite GDS108-4689, PS-16A; phlogopite HS23, NMNH12458.)

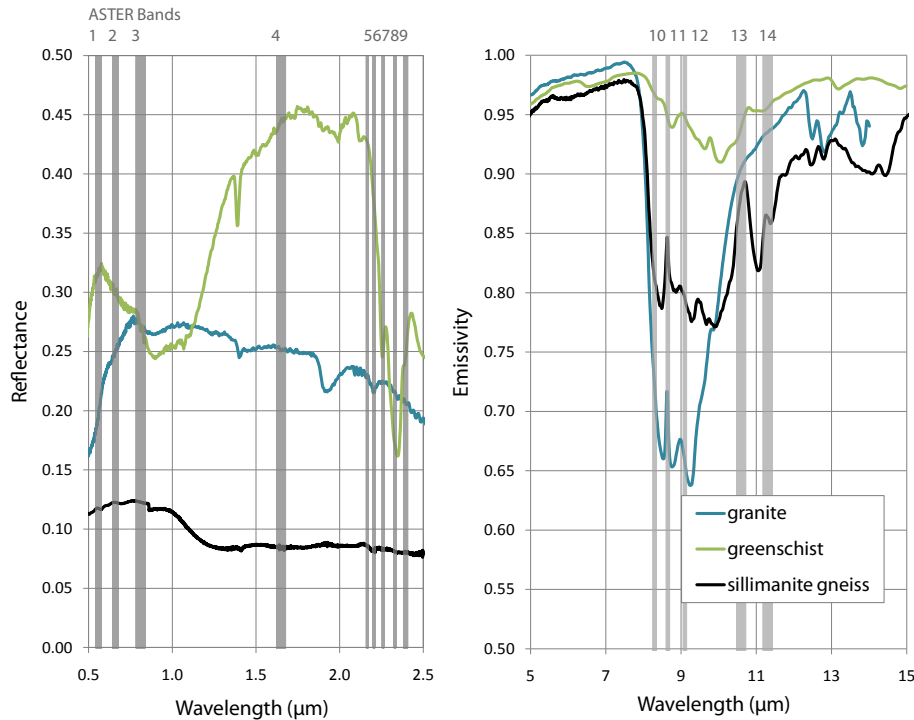


Figure A2. Reflective (VNIR-SWIR, left plot) and emissive (TIR, right plot) rock spectral signatures are displayed with ASTER multispectral band wavelength positions over plotted in gray. Emissivity values were calculated using Kirchoff's Law ($E = 1 - R$) where E is emissivity and R is reflectance. Note that measurements are from the USGS spectral library of specimens collected in different regions, and measured with differing laboratory conditions. Hence, signatures should be visualized with respect to general shape and potential characteristic features). (ASTER rock spectral library references: granite NMNH113640-17, greenschist 392, sillimanite gneiss Ward80.)

Optical remote sensing of debris covered glaciers

K. A. Casey et al.

Title Page

Abstract Introduction

Conclusions References

Tables Figures

◀ ▶

◀ ▶

Back Close

Full Screen / Esc

Printer-friendly Version

Interactive Discussion

